# Intelligent energy management scheme for a hybrid microgrid using machine learning

**Prepared by:**
Julian Banks (BNKJUL001)

**Prepared for:**
Professor Sunetra Chowdhury
Department of Electrical Engineering
University of Cape Town

Submitted to the Department of Electrical Engineering at the University of Cape Town in partial fulfilment of the academic requirements for a Bachelor of Science degree in Mechatronics Engineering

October 25, 2023

# Declaration

1. I know that plagiarism is wrong. Plagiarism is to use another's work and pretend that it is one's own.
2. I have used the IEEE convention for citation and referencing. Each contribution to, and quotation in, this report from the work(s) of other people has been attributed, and has been cited and referenced.
3. This report is my own work.
4. I have not allowed, and will not allow, anyone to copy my work with the intention of passing it off as their own work or part thereof.

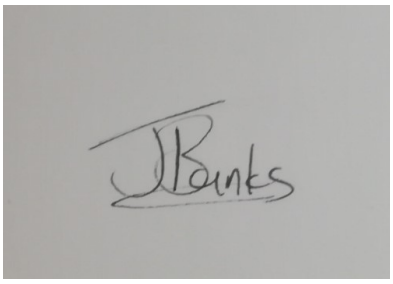

October 25, 2023

Julian Banks

Date

# Acknowledgements

No man is an island entire of itself; every man is a piece of the continent, a part of the main.

—*John Donne*

# Abstract

With the just energy transition, there has been an uptake on the usage of microgrids as a method of including renewable energy. A key factor in reducing the running costs and improving power quality in a microgrid is the energy management strategy.
This report explores the possibility of an autonomous agent to perform energy management for a microgrid that has both an AC and a DC load, known as a hybrid microgrid.
The task of energy management was broken into three main sections. Obtaining load forecasts using predictive machine learning techniques, obtaining generation forecasts from weather data or service providers, and finally training an agent to perform energy management through simulations using reinforcement learning techniques.
Due to the inherent randomness in load usage the predictive results over the a full 24 hours did not prove to be extremely accurate with the best machine learning algorithm achieving 20% Mean Absolute Percentage Error (MAPE). However, due to the strong temporal nature of load profiles the prediction for 1 hour ahead was able to achieve 5% MAPE. TALK ABOUT AGENTS RESULTS NEXT.

Results: Summarise the key findings or results of the study. Highlight the most significant outcomes or discoveries. Use quantitative data, if applicable, to support your statements.

Conclusions: Present the main conclusions drawn from the study. What are the implications of the findings? How do they relate to the research objectives?

Significance or Importance: Discuss the significance or importance of the research within the broader scientific context. Explain why the study is relevant and what it adds to existing knowledge in the field.

# Contents


**Abbreviations** **viii**

**1 Introduction** **1**
1.1 Background to the study . . . 1
1.2 Objectives of this study . . . 1
1.2.1 Tasks to be investigated . . . 1
1.2.2 Purpose of the study . . . 2
1.3 Scope and Limitations . . . 2
1.4 Plan of development . . . 2

**2 Literature Review** **3**
2.1 Hybrid microgrids . . . 3
2.2 Energy management techniques . . . 6
2.3 Application of machine learning to energy management. . . . 9
2.3.1 Machine learning as a tool for prediction. . . . 9
2.3.2 Machine learning as a tool for scheduling . . . 10
2.4 Conclusion . . . 11

**3 Theory** **12**
3.1 Machine learning theory for forecasting . . . 12
3.1.1 Analysis of potential regression techniques . . . 12
3.1.2 Auto-regressive Models . . . 12
3.1.3 Neural Networks . . . 14
3.1.4 Long Short Term Memory Networks . . . 15
3.2 Data processing theory . . . 15
3.2.1 Rescaling . . . 15
3.3 Reinforcement learning theory . . . 16
3.4 Machine Learning software . . . 17
3.4.1 MATLAB . . . 17

**4 Data collection and preprocessing** **19**
4.1 AC and DC load data . . . 19
4.1.1 Cleaning load data . . . 20
4.2 Time of use rates . . . 21
4.3 Loadshedding 2022 schedule . . . 22

**5 Microgrid design** **23**
5.1 Design of Hybrid Microgrid . . . 23

5.1.1 Homer PRO Input . . . 24
5.1.2 Homer PRO output . . . 25
5.1.3 Final grid parameters . . . 26
5.2 PV and wind generation data . . . 27
5.2.1 Simulated generation data . . . 27
5.2.2 Generation forecasting note . . . 28

**6 Load forecasting** **29**
6.1 Exploratory Data Analysis . . . 29
6.1.1 Feature Selection . . . 31
6.2 Fitting LSTM model . . . 33
6.2.1 Data Preparation . . . 33
6.2.2 Normalisation . . . 33
6.2.3 LSTM configuration and training . . . 34
6.2.4 Forecasting method . . . 35
6.3 Fitting ARIMA model . . . 36
6.3.1 Data Preparation . . . 36
6.3.2 Determining Model Parameters . . . 36
6.3.3 Training the model . . . 37
6.3.4 Forecasting method . . . 38
6.4 Fitting SARIMA model . . . 38
6.4.1 Determining Parameters . . . 38
6.4.2 Training Model . . . 39
6.4.3 Forecasting method . . . 40
6.5 Fitting ANN model . . . 40
6.5.1 Data Preparation . . . 40
6.5.2 Training Model . . . 41
6.5.3 Forecasting method . . . 41

**7 Load forecasting results and discussion** **43**
7.1 Results . . . 43
7.1.1 Metrics of Evaluation . . . 43
7.1.2 Forecasting Procedure . . . 43
7.1.3 Evaluation of the LSTM model . . . 44
7.1.4 Evaluation of the SARIMA model . . . 45
7.1.5 Evaluation of the Neural Net model . . . 46
7.2 Load forecasting Discussion . . . 47
7.2.1 Model performance . . . 47
7.2.2 AC and DC load variablity . . . 47
7.2.3 Final load forecasting model . . . 48

**8 Energy management agent** **49**
8.1 Reinforcement learning applied to EMS . . . 49
8.2 Simplified environment . . . 50

8.2.1 Environment . . . 51
8.2.2 Results of EMSv0.1 . . . 53
8.3 Development of the Environment and Agent . . . 54
8.3.1 Implementation of a hybrid grid and load shedding . . . 54
8.3.2 Implementation of a demand charge and continuous action space. . . . 56
8.4 Final RL implimentation . . . 57
8.4.1 Environment . . . 57
8.4.2 Observation space . . . 58
8.4.3 Action space . . . 59
8.4.4 Reward . . . 59
8.4.5 Step function . . . 60
8.4.6 Training method . . . 60

**9 Results & Discussion** **61**
9.1 Evaluation metrics . . . 61
9.2 Energy management system results . . . 61
9.2.1 Performance of the agent with no loadshedding . . . 61
9.2.2 Performance of the agent with loadshedding . . . 62
9.3 Final energy management discussion . . . 64

**10 Conclusions and Recommendations** **65**

**Bibliography** **66**

**A Additional Files for Design of Hybrid Microgrid** **68**

**B Additional information for reinforcement learning implementation** **69**

**C Addenda** **72**
C.1 Ethics Forms . . . 72

# Abbreviations

**ACF** Auto Correlation Function

**ANN** Artificial Neural Network

**AR** Auto Regressive

**ARIMA** Auto Regressive Integrated Moving Average

**AutoML** Automated Machine Learning

**CEEMDAN** Complete Ensemble Mode Decomposition with Adaptive Noise

**CNN** Convolutional Neural Network

**DDPG** Deep Deterministic Policy Gradients

**EMS** Energy Management System

**ESS** energy storage system

**GRU** Gated Recurrent Unit

**IMF** Intrinsic Mode Functions

**KPSS** Kwiatkowski–Phillips–Schmidt–Shin

**LSTM** Long Short Term Memory

**MAPE** Mean Absolute Percentage Error

**MDP** Markov Decision Process

**ML** machine learning

**MPPT** maximum power point tracking

**NPC** Net Present Cost

**PACF** Partial Auto Correlation Function

**PER** Prioritized Experience Replay

**PID** Proportional, Integral and Derivative

**PPO** Proximal Policy Optimisation

**PV** photovoltaic

**RL** Reinforcement Learning

**RMSE** Root Mean Square Error

**RNN** Recurrent Neural Network

**SAC** Soft Actor Critic

**SARIMA** Seasonal Auto Regressive Integrated Moving Average

**SARIMAX** Seasonal Auto Regressive Integrated Moving Average with Exogenous Variables

**TOU** Time of Use

**UCT** University of Cape Town

**WNN** Wavelet Neural Network

# Chapter 1

# Introduction

## 1.1 Background to the study

A very brief background to your area of research. Start off with a general introduction to the area and then narrow it down to your focus area. Used to set the scene . This project combines two very important fields of study. Due to the current climate crisis that the globe is facing, there has been a large uptake in renewable energies. A major feature in renewable integration is the microgrid entity. Microgrids are typically made of various forms of distributed generation, one or more loads, an energy storage system (ESS) and they usually have the ability to operate in islanded or grid connected modes. Finally, an Energy Management System (EMS) is employed to manage the flow of power between the various components.
Finding the optimal way to implement the energy management system can lead to increased renewable penetration, increased power quality and cost savings. This is where the second field of research enters. With recent advancements in machine learning autonomous agents have become more capable. Machine learning algorithms can learn patterns and use various regression techniques to make predictions of future values of time series. While deep reinforcement learning has shown good results in training an agent to navigate an environment through reward based simulations. Applied in the context of energy management, an autonomous energy management system could make predictions of future load and generation values, and then proceed to take what it determines to be the best action based.

## 1.2 Objectives of this study

### 1.2.1 Tasks to be investigated

This study sets out to determine if an autonomous agent can be trained to make load predictions and then use these predictions to perform energy management. The success of the agent will be measured by cost savings, renewable penetration and power quality.

The study has four key tasks were derived from insights gained during the literature review. Each key task is detailed in its own chapter.
The framework is structured as follows.

1. **Data collection and preprocessing**: This crucial step outlines the process of finding the necessary data to model the hybrid microgrid.

2. **Microgrid design method**: Once the data is collected, this section details how HOMER Pro

will be utilised to design the hybrid microgrid.

3. **Load forecasting approach**: This section delves into machine learning theory, particularly focusing on time-series forecasting, to inform the approach to load forecasting. The goal is to explore and discern the most suitable models for accurate load forecasting.

4. **Generation forecasting approach**: This section briefly outlines how generation forecasts can be determined. It explores paid services such as SolarGIS, using weather predictions and associated calculations.

5. **Autonomous energy management system**: The culmination of the methodology is determining the best reinforcement learning approach to train an autonomous energy management agent. This process will make use of the designed microgrid, the load and generation forecasts.

### 1.2.2 Purpose of the study

South Africa is currently in an energy crisis that will require the wide spread installation of renewable energy. This study aims to explore possibilities of using machine learning as a method of providing adaptable and autonomous energy management systems to these microgrids. With the aim of reducing the operating costs thereby making the endeavour more affordable.

## 1.3 Scope and Limitations

Scope indicates to the reader what has and has not been included in the study. Limitations tell the reader what factors influenced the study such as sample size, time etc. It is not a section for excuses as to why your project may or may not have worked.

In order to ground the projects scope, a building on University of Cape Town (UCT) upper campus was chosen as the load for the microgrid to be modelled from. This buildings real AC load data was used as the microgrids AC load. Unfortunately, it was not possible to access a real world DC load, instead a load profile was found from an open source data set. The design of the microgrid was assisted by Homer PRO software and simply. All predictions and energy management was performed at hourly intervals. The load predictions were limited to 24 hour ahead as this is sufficient for localised energy management. Generation forecasts were not calculated in this project as there are already multiple specialised services that provide generation forecasts.

## 1.4 Plan of development

The report begins by developing an understanding of microgrids and EMS's through a literature review. It then goes on to develop the necessary machine learning techniques that will be employed.
The methodology then outlines the collection of data which is used to design the hybrid microgrid that is used as a testing base for the EMS. Regression machine learning techniques are then used to generate a model that can produce load forecasts. A section then briefly explains how generation forecasts could be obtained from weather forecasts or from specialised services. Finally the results from the previous two sections are used to train an agent using reinforcement learning to perform energy management for the hybrid microgrid. TALK ABOUT RESULTS AS WELL

# Chapter 2

# Literature Review

There has been extensive research into hybrid microgrids, their configuration, optimisation and interconnectivity with a utilities grid.

To remain within the scope of this report the literature review will explore three key topics related to hybrid microgrids. Namely, configurations of hybrid microgrids with both AC and DC subgrids. A look into contemporary energy management techniques for systems with less than 1MW generation capacity. Lastly, it will explore how machine learning has been applied to the energy management of hybrid microgrids.

## 2.1 Hybrid microgrids

Microgrids have gained traction as new forms of renewable energy generation have been developed and political pressure to decarbonise energy has increased. Microgrids are typically low-voltage networks employing distributed generation to meet local demand. Typical forms of generation include solar photovoltaic (PV), wind and diesel. Microgrids are usually equipped to operate in islanded or grid-tied modes. If they are required to reliably provide power to a load during islanded modes it is also necessary to include energy storage systems in the design.

Microgrids often use diesel generators to ensure energy security. This is due to the intermittent nature of popular renewables such as solar and wind. Additionally, it is typically costly to install an energy management system that is large enough to ensure energy security in the event of the microgrid operating in islanded mode. Diesel is a potent fossil fuel and an unattractive option in an energy system for the future. Alternatives such as bioenergy that implement a waste-to-energy cycle using biomass or bio-wast have been proposed. These have been excluded from this study as the composition of the hybrid microgrid is not the main focus, however, it would be interesting to explore their integration into microgrids in the future. [1]

Since microgrids function in a localised area they require integrated control systems to perform energy management, voltage regulation and frequency regulation. [2] When considering common microgrid control algorithms, the majority have been designed to operate AC microgrids. This is largely due to all major transmission lines being AC. The rise in DC load from consumer electronics and the growth of electric vehicles coupled with the DC nature of renewables such as PV creates a good argument for the installation of DC subgrids in a hybrid microgrid. Other advantages of DC subgrids include being free from frequency, power factor and phase sequence issues.[3]

A hybrid microgrid composed of both AC and DC subgrids will allow for loads to be met with fewer conversion stages if both AC and DC generation is employed. As the AC load will primarily be met by the AC generation and the DC load will primarly be met by the DC generation.
This will reduce power conversion losses and lower the number ac-dc and dc-ac converters needed. [2] Bidirectional converters can be used to control the flow of active power between the AC and DC subgrid. This allows one subgrid to become a load or a source while the other subgrid becomes the opposite. This means that only the imbalance will need to pass through the converter, thus lowering the converter losses. However, the balancing of loads needs to be done in proportion to the generation capacity of each subgrid. This can be achieved by using a normalisation process that is explained in more detail in the energy management section of the literature review. [4]

Various configurations and topologies of hybrid grids have been explored in the literature. The two main types are coupled AC hybrid microgrids where the AC subgrid is attached to the utility grid via transformers. The second type is decoupled AC hybrid microgrids where the DC subgrid is connected to the grid and the AC subgrid connects to the DC subgrid. [5] The main advantage of a couple AC hybrid microgrid is that there are fewer power conversion stages as only a transformer is required to connect the subgrid to the utility grid. Additionally, the AC network is connected to the utility grid when it is operating in grid-connected mode, fixing the voltage and frequency to that of the grid. This removes the need for vigorous frequency control etc. The main advantage of the decoupled AC configuration comes from the inherent control provided by the power converters between the utility grid and the microgrid. They allow for accurate tracking of power flow and makes fault detection easier. [5]

Coupled ac configurations can be further broken down into partially isolated and completely isolated systems.

Partially isolated systems consist of a low-voltage AC subgrid connected to the utility grid via a transformer and a low-voltage or medium-voltage DC subgrid connected to the utility grid via a power converter. This gives the advantage of requiring a power converter with a lower rating since it does not need to handle the power flow of the AC grid. However, it means that there is no galvanic isolation of the DC subgrid. Figure 2.1 outlines the configuration.

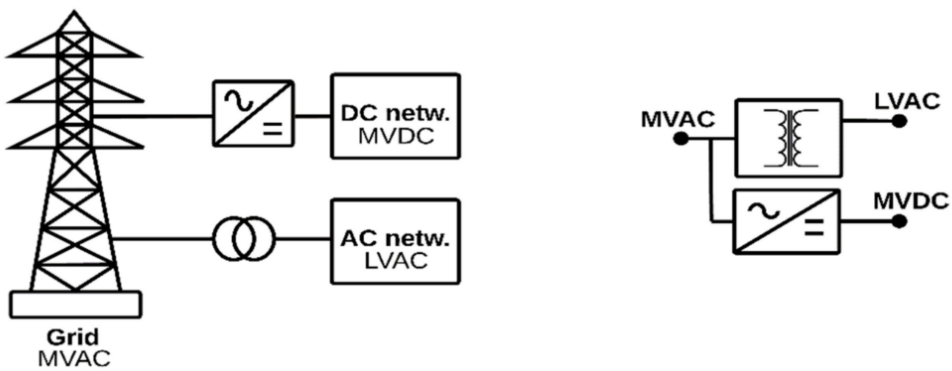


Figure 2.1: Coupled AC microgrid in partially isolated configuration. (source: [6])

Completely isolated systems consist of an AC subgrid that connects to the utility grid via a transformer

and a DC subgrid that connects to the AC subgrid via a power converter. This means that the entire microgrid experiences galvanic isolation. This is useful for connections that have a high risk of experiencing faults. However, the transformer will require a higher power rating as it needs to be able to handle the power flow from both the AC and the DC subgrid. Figure 2.2 outlines the configuration.

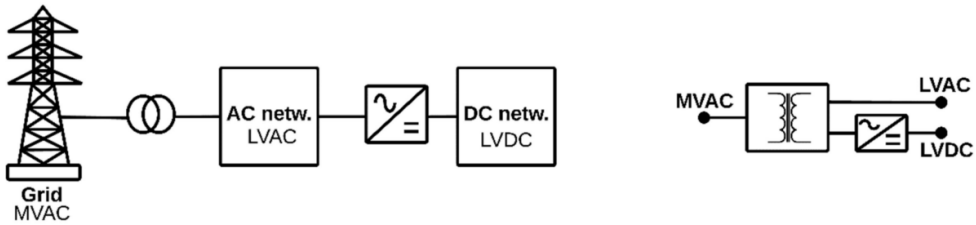


Figure 2.2: Coupled AC microgrid in completely isolated configuration. (source: [6])

Decoupled hybrid microgrids can be broken up into three main groups. Two-stage completely isolated, Two-stage partially isolated and Three-stage partially isolated. This review will not look into the Three-stage partially isolated system as it is typically used on larger scale solar or wind farms.

The two-stage completely isolated configuration can be seen in Figure 2.3. This configuration benefits from complete galvanic isolation due to the transformer placed between the utility grid and the AC/DC converter. This makes it more suitable to scenarios expecting a higher level of grid faults.

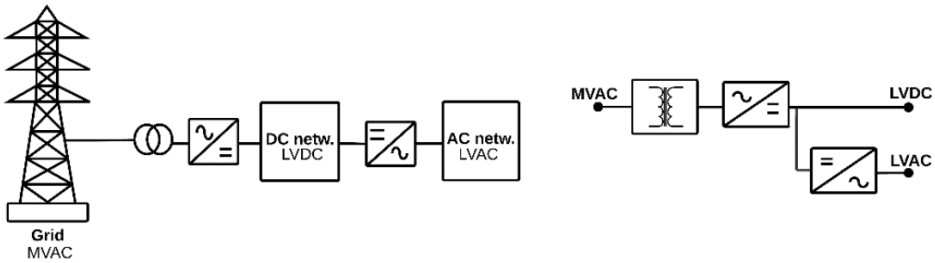


Figure 2.3: Decoupled AC microgrid in completely isolated configuration. (source: [6])

The two-stage partially isolated configuration can be seen in figure 2.4. This major difference in this configuration is that the transformer is moved and placed inbetween the DC subgrid and the AC subgrid. The advantage of this is that the transformer's power rating can be lower than in the completely isolated decoupled scenario.

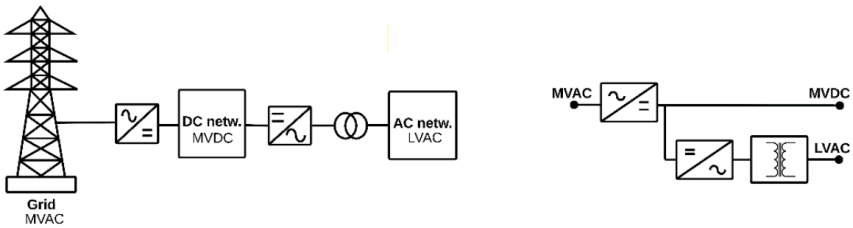


Figure 2.4: Decoupled AC microgrid in a partially isolated two-stage configuration. (source: [6])

What none of these configurations have explicitly included is an ESS. Due to the intermittent nature

of renewables and the likelihood of load shedding, it will be essential to integrate an ESS into the system. An ESS will be responsible for storing energy during periods of excess generation or in off-peak grid times. It can then supplement the supply at times when the load is higher than the generation. This typically requires a bi-directional DC-DC converter to help with stabilising the voltage in the DC subgrid [7]. The development of ESS is currently a very active space in research, however, the accepted industry standard is currently the lithium ion battery due to its ability to withstand a high number of cycles, fast charging and discharging and high depth of discharge.

It is worth noting that the composition and design of microgrids are based on too many factors for a universal approach to be viable. Each design needs to be tuned for its environment and application related parameters. In [8], this is handled by employing a 2 layered Multi-criteria decision-making model. This first calculates the weights of each criterion and then uses ranking methods to determine the optimum compromise. HOMER software was employed to test simulations of various configurations.

From the available literature the usage of HOMER Pro to design microgrids has been widely accepted. Common sources of DC generation such as solar PV can be used to meet DC loads and to charge DC ESS such as lithium ion batteries. Wind turbines can be configured to provide AC or DC power depending on their design and construction, making them a flexible option for the design of a hybrid microgrid. Diesel generators are commonly used to provide power security and produce AC power. While there are various topologies available for hybrid microgrid's, the most general one appears to be the coupled AC configuration.

## 2.2 Energy management techniques

A crucial element of any microgrid is its control and EMS. The power flow between the distributed generation and the loads, the flow of power between the AC and the DC subgrids, the management of energy storage systems and the switching between islanded and grid-tied operations are just some of the necessary control systems. Additionally, the implemented control system needs to be flexible and able to handle any number of operating points due to the unreliable nature of renewables. [9]

In [7] the control system is split into three parts, the energy management system, the supervisory control and the local control. The energy management system schedules the power generation according to a day ahead schedule. This comes from a prediction of weather patterns and load profiles. The supervisory control manages the discrepancy between the scheduled power and the actual power used and generated. The local control system manages the voltage, current, and frequency of the microgrid. The results showed that the combined control system was effective at reducing costs and increasing the reliability of the hybrid microgrid. The proposed system in [7] includes solar PV and hydrogen fuel cells, the local control of each of these systems is performed by a Proportional, Integral and Derivative (PID) controller. The fuel cell setup uses a reference voltage and increases the generation whenever the voltage at the terminals falls below the terminals and vice versa. The solar PV system uses maximum power point tracking (MPPT) to optimise generation from the solar PV panels and the output of the MPPT is used as the input to the PID loop.

Matching controllable loads to peaks in power generation was explored in [10]. This was done by using predictions of the upcoming wind patterns and moving a controllable load to be connected during

periods of peak production. An example of this could be scheduling the ESS to be charged at a point of peak power production based on a weather prediction. The study found that the method showed an increase in the state of charge of the energy storage system as well as a decrease in the usage of the supplementary diesel generator. However, this method relies on accurate forecasting of weather.

Droop control is a well-established form of control in AC microgrids. In [4] its use was extended to control a hybrid microgrid with both AC and DC subgrids. Droop control is achieved by determining the droop co-efficient for each energy source. In an AC microgrid, each source has two droop co-efficients, one for voltage and one for frequency. These coefficients are given by the equation 2.1 and equation 2.2, where the x represents the source in the AC subgrid. $f^*$ and $V^*$ are the sources reference frequency and voltage while $f'$ and $V'$ are the maximum no-load voltage and frequency. The droop co-efficients are represented by $m_x$ and $n_x$, these are calculated according to 2.3 and 2.4. The $P_a$ and $Q_a$ terms come from locally measured power and reactive values.

$$f_x^* = f_x' + m_x P_{a,x} \tag{2.1}$$

$$V_{a,x}^* = V_{a,x}' + n_x Q_{a,x} \tag{2.2}$$

To then share the load in proportion to the rated capacity of the source the droop coefficients are used together with the sources rating, given as $S_{a,x}$. These values are used to satisfy the equations 2.3 and 2.4 balancing the load proportionally between the sources.

$$m_1 S_{a,1} = m_2 S_{a,2} = ... = m_x S_{a,x} \tag{2.3}$$

$$n_1 S_{a,1} = n_2 S_{a,2} = ... = n_x S_{a,x} \tag{2.4}$$

This was done for all of the sources in the AC subgrid. For the sources in the DC subgrid, the process was slightly different as there is no frequency component. Instead the equation 2.5 was used to calculate the droop coefficient, where $V_{d,y}'$ is the maximum output of a source under no load. And $v_y$ is the droop coefficient. The proportional load sharing is then managed by the equation 2.6.

$$V_{d,y}^* = V_{d,y}' + v_y P_{d,y} \tag{2.5}$$

$$v_1 S_{d,1} = v_2 S_{d,2} = ... = v_x S_{d,x} \tag{2.6}$$

In [11], the energy management system is implemented logically by using a set of conditions. The conditions include production from the microgrid, the price of grid electricity, the load and the state of charge of the energy storage system. It is assumed that all of the loads and generation values are known at all times. This is a high-level form of control where the main priority is to keep the flow of power balanced between the loads and the sources. The rule-based control scheme can be visualised using a flow chart, an example is given in figure 2.5. The scheme was successful in balancing the loads and improving the performance of the system theoretically. However, it does not address how the actual control will be implemented, the high level of information that all of the conditions require implies that the system will require many sensors and a centralised control unit. These are factors that greatly affect the cost and reliability of the system.

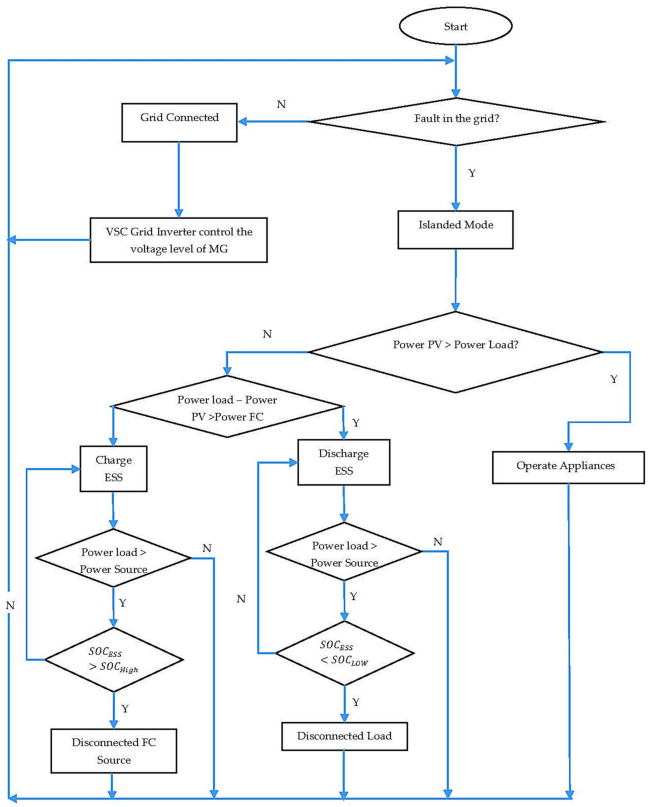


Figure 2.5: A simple rule based scheme for energy management [7].

This issue of reducing the many sensors required to monitor every load and form of generation is tackled in [12]. The approach focuses on the voltage of the DC-link. Control is performed by measuring the voltage of the DC link and using PI controllers to keep the voltage at a constant reference voltage. This is done by injecting power or drawing more power (selling it to the grid or storing it). A rule-based control scheme is still implemented at this stage. However, now the only inputs that are required for the controller are current through the DC-link (derived from the voltage), a boolean for whether the microgrid is islanded or not, a boolean for whether it is a peak pricing time or not and the state of charge of the batteries. [12] also includes supercapacitors to help smooth the transients and reduce the stress on the batteries. An important consideration that [12] brings up is the operation of the hybrid in off-MPPT mode. Typically MPPT is used to draw the maximum power from a PV system. However, if generation exceeds the load, the energy storage system is fully charged and the microgrid is in islanded mode then there is nowhere for the excess power to go and the PV system should not track the maximum power point.

Similar to a rule-based scheme, [13] uses states to implement supervisory control. In this case, every combination of loads and generation is assigned to a state. The controller then decides what state to put the system into. The states have entry conditions that are based on the available power of the sources and the required powers of the loads. The states have been chosen to maximise the renewable penetration and a diesel generator is only used to prevent load shedding if the wind and PV generation cannot meet the demand and the batteries are fully discharged. The supervisory control is shown to operate as expected and successfully change states to match loads. However, the performance is not compared to a benchmark so it is difficult to judge how effective the energy management system truly was. An important practical note the [13] brings up is the need to ensure impedance and voltage

matching of converters. For example, if the DC subgrid is connected to the PV panels via a DC/DC converter and to the AC subgrid via an AC/DC converter then any mismatch between these converters will negatively affect power quality.

The energy management system that [14] uses is for a simple microgrid. The researchers approach the problem from an angle of optimisation and use integer linear programming to determine the optimal method of control. The microgrid in question contains a PV system, a wind turbine and an ESS of lead-acid batteries. The energy management system uses weather and load profile predictions along with grid pricing of electricity to schedule the state of charge of the batteries and to minimise the objective function. The objective function is designed to minimise operating costs. For cases when the load was low enough for the microgrid to never need to buy from the grid, it was found that using MPPT controllers was slightly more effective than the optimised energy management system. However, in cases when the microgrid was required to buy electricity from the grid the optimised energy management system outperformed the MPPT controllers as it was able to schedule the purchase of electricity during off-peak periods at a lower price.

Machine learning is able of producing agents that undertake decision making, understand relationships and can make predictions. From its strengths it is clear that it lends itself to a high level form of energy management.

## 2.3 Application of machine learning to energy management.

### 2.3.1 Machine learning as a tool for prediction.

For renewables that are heavily dependent on the weather, such as wind or PV, an accurate forecast of generation capacity is vital. Using machine learning techniques to make these predictions has been a growing field of study.

In [15], researchers use a Convolutional Neural Network (CNN) combined with a Gated Recurrent Unit (GRU). Weather data in the form of temperature, humidity, air pressure, and air density were collected at the site of renewable energy sources. It is interesting that they have chosen to measure pressure and density rather than wind speed. The collected data was used by the CNN and GRU algorithms to predict weather patterns. After the method was refined and an attention mechanism was added to the network the best result achieved was 17.99% Mean Absolute Percentage Error (MAPE) for a day ahead prediction. In [16] a similar combination of CNN and GRU was used to forecast price, wind speed and solar irradiation. However, much more accurate results were reported with MAPE values as low as 3.6% for wind speed and 5.47% for solar irradiance. However the researchers have not been clear about the forecast period, the forecast seems to only be one hour ahear which would explain the low MAPE values.

A feature that machine learning has shown promise in is the prediction of load profiles. If it is possible to accurately perform next-day load prediction it will be possible to implement an informed energy management strategy. In [17], this idea is explored and showed promising results. Various combinations of Artificial Neural Network (ANN), Wavelet Neural Network (WNN) and Kalman Filters are used to test the accuracy of load forecasting using neural networks. It was found that using a WNN and

then feeding the results into an ANN in a hybrid neural network produced the best results. Given the necessity for an intelligent grid to be able to accurately schedule production, accurate predictions of loads will be incredibly valuable. The work done in [15] also used a combination of algorithms, a Complete Ensemble Mode Decomposition with Adaptive Noise (CEEMDAN) and a GRU was trained to predict the day ahead electrical load. An interesting property of the CEEMDAN network is that it can break the data into Intrinsic Mode Functions (IMF)s. This allows the model to identify the slower-moving and dominant IMFs. These are easier to predict and help to reduce the prediction error. The MAPE error was lowered to only 2.88%, although this appears to be the error when predicting one timestep ahead rather than a full hourly day ahead prediction.

An important argument is raised by [18], supervised learning can provide a high level of accuracy and can be tempting when research is carried out with a defined model and set of data. However, this will create models that are case-specific and not easily adaptable to the real world, unless of course a huge amount of data can be accessed. A preferable method of training could instead include reinforcement learning. In [18] the energy management system is split into two main tasks, prediction of generation and load and generation scheduling. The day ahead prediction of the energy generation and load is performed by Automated Machine Learning (AutoML) combined with Prioritized Experience Replay (PER). The results boast a high level of accuracy with a MAPE of 8% for the PV prediction, 7% for the wind prediction and 1.8% for the load prediction. The paper also goes on to use linear programming to find the optimal scheduling scheme for the system once the predictions have been made.

### 2.3.2 Machine learning as a tool for scheduling

In [19] the energy management problem is simplified to finding the best combination of energy sources that should meet the current load. The scheduling predictions were simplified further to be based on 4 inputs, namely, the hourly load demand, the temperature and two binary values for the availability of sun and wind. This accounts for varying loads but does not account for varying levels of wind or solar irradance as both factors have been simplified to a boolean. The output of the neural network was divided into classes. Where each class represented a different configuration of active energy sources. Four neural net algorithms were tested. All of the algorithms were found to perform well however the best one in terms of accuracy and performance was the Decision Tree algorithm. The Decision Tree algorithm is used to solve classification and regression problems. A major advantage of the algorithm is that it does not require scale normalisation and that it can operate with a range of attributes.

The scheduling challenge is optimised in [20] by transforming the problem into a Markov Decision Process (MDP). A Q-learning algorithm is then chosen due to its suitability for handling MDP problems to tackle the issue of energy storage management. The paper found varying results with the six variations of the algorithm that it tested. Unfortunately, none of them could match the theoretical limit that was calculated by the mixed integer linear programming method. However, they were able to converge on their result more quickly and were thus computationally cheaper.

Find a paper that talks about reinforcement learning.

## 2.4 Conclusion

The topic of hybrid microgrids has been produced many research papers with varying approaches. The configuration of each microgrid will vary depending on the environment meaning that solutions have to be adaptable and fitted on a use case basis. However, there are some universal trends, such as the need for energy storage and technologies such as wind and solar generation.
Energy management in microgrids provides an opportunity to optimise the renewable penetration and operating cost of a microgrid while increasing energy security.

Machine learning presents a promising opportunity to design a flexible and easily deploy-able energy management agent. That is able to not only make weather and load forecasts but able to take actions in real time to perform energy management.

In conclusion the key areas that have identified from the literature as areas that machine learning can be applied to energy management is in load forecasts, generation forecasts and scheduling of purchases in a microgrid.

# Chapter 3

# Theory

## 3.1 Machine learning theory for forecasting

This section aims to outline and develop the machine learning approach that will be used to produce load forecasts. Producing accurate load forecasts was identified as a key challenge in energy management. Load forecasts will be used to assist the agent in performing energy management.

The core of this task is to forecast the load values for the upcoming 24 hourly timesteps. This is called a day ahead forecast. This type of timeseries analysis and prediction typically uses regression learners.

### 3.1.1 Analysis of potential regression techniques

Regression models are typically use supervised training to fit models. This means that historical predictors and targets are used in pairs to train models. The primary objective of most supervised learning methods is to learn a mapping from a set of input features to a target response variable. The model aims to learn relationships that can be applied to unseen data to make predictions.

Regression models typically aim to predict a continuous numerical value. This is done by plotting a line of best fit or a curve to the data. Typically a trained regression algorithm is evaluated using the variance, bias and error. A high variance can lead to overfitting while a high bias can lead to underfitting. Regression can be linear (one input to one output), multiple (many inputs to one output), or multivariate (many outputs). Linear regression is limited to plotting linear equations and works best when predictors are independent and uncorrelated to each other. For non-linear data, it is necessary to use polynomial regression. Polynomial regression is able to plot curves between data. In order to avoid overfitting the degree of the polynomial needs to be tuned. Regularization is also used to reduce the potential for overfitting by adding a penalty term to the cost function. The ridge and lasso regression techniques each make use of their own formulas to perform regularisation as can be seen in Figure 3.1.

### 3.1.2 Auto-regressive Models

Auto Regressive (AR) models are a widely used time series forecasting models that work by capturing and fitting different aspects of temporal data patterns. The key feature of a pure AR model is that the future values of a time series depend only on its past values (known as lags).

$$Y_t = \alpha + \beta_1 Y_{t-1} + \beta_2 Y_{t-2} + ... + \beta_p Y_{t-p} + e \tag{3.1}$$

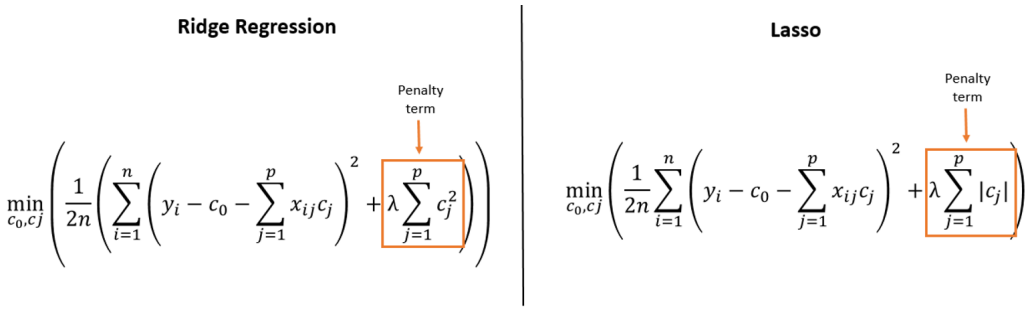


Figure 3.1: Ridge vs. Lasso regularization techniques. (source: [21])

In equation 3.1, $Y_{t-1}$ is the first lag, $\beta_1$ is the coefficient of the first lag term, $\alpha$ is the model's intercept term and $e$ is the error term. The index 'p' is what defines the order of an AR model. It determines how many lags of the function will be used as predictors (how many past values contribute to the future value).

AR models are a fundamental component of models such as Auto Regressive Integrated Moving Average (ARIMA),Seasonal Auto Regressive Integrated Moving Average (SARIMA) amd Seasonal Auto Regressive Integrated Moving Average with Exogenous Variables (SARIMAX).

#### 3.1.2.1 ARIMA

ARIMA adds two important features to AR models. Firstly it uses differencing to make the time series stationary. Differencing entails subtracting the previous value from the current value and can be performed multiple times. This removes a trend from data, for example if every sample increases by 5 units, then the mean of the timeseries would change with time. By subtracting the previous value from the current value the resulting series would constantly be 5, and its mean would not change with time. This helps it to model real-world time series data. Secondly, it uses a moving average (MA) component to make the model dependent on its past forecasting errors. ARIMA models can be used to model any 'non-seasonal' time series that shows patterns and is not a random white noise function. Therefore an ARIMA model can be defined as a time series that may have been differenced to make it stationary and can be described by a combination of the equation for AR and MA.

$$Y_t = \alpha + +\beta_1 Y_{t-1} + \beta_2 Y_{t-2} + ... + \beta_p Y_{t-p} + e_t + \phi_1 e_{t-1} + \phi_2 e_{t-2} + ... + \phi_q e_{t-q} \tag{3.2}$$

The first half of equation 3.2 is identical to equation 3.1 for AR models while the terms with $\phi_i e_{t-i}$ contribute the moving average. Each error term comes from the error of the respective lag term, $\phi$ is the coefficient for that error term and the index 'q' defines how many error terms are included in the equation.

As mentioned earlier, it may be necessary to difference a time series to make it stationary. It is optimal to perform the minimum differencing required to achieve a time series that is near-stationary. This means it stays close to a defined mean and the Auto Correlation Function (ACF) plot tends to zero within a reasonable frame.
If many of the lag terms show a positive autocorrelation then the series should be differenced further. Conversely, if the first lag experiences a negative autocorrelation then the series may be over-differenced. Determining the number of 'p' or AR terms can be determined by examining the Partial Auto Correlation

Function (PACF). The PACF helps to convey the correlation between a specific lag and the series, which helps to determine whether the lag is needed in the AR term or not. A good starting estimate is to set the order of the 'p' term to equal the number of lags that are above the significance limit in the PACF plot.

The moving average or the 'q' term can be determined by looking at the ACF. Similarly to the 'p' term, the 'q' term can initially selected by setting it equal to the number of lags that are above the significance limit of the ACF.

Once these initial terms have been chosen it will likely be necessary to tune them after defining and training the model. This is done by inspecting the coefficients and the significance of each term. The residuals of the model can also help to show a good fit, residuals with no patterns and a constant mean and variance are ideal.

In summary, an ARIMA model can be used to forecast values of a non-seasonal time series and is characterised by three terms.
The 'p' term is the order of the AR component.
The 'q' term is the order of the Moving Average (MA) component.
The 'd' term is the number of times the series needs to be differenced to make the series stationary.

#### 3.1.2.2 SARIMA

A possible issue with using an ARIMA model is that it does account for seasonality. If a time series displays seasonal trends then the standard method of differencing will not make the series stationary. Seasonal differencing works by subtracting the value from the previous season instead of from the previous term.

SARIMA models have an additional set of parameters that describe the seasonality.
'P' is the order of the Seasonal Auto Regression (SAR).
'D' is the order of the seasonal differencing.
'Q' is the order of the Seasonal Moving Average (SMA).
Additionally, the frequency of the seasonal pattern needs to be defined.

#### 3.1.2.3 SARIMAX

SARIMAX adds in an external predictor called an exogenous variable. This can help to improve the forecast accuracy by including external factors that will influence the time series. The exogenous variable must be known during the forecast period.

### 3.1.3 Neural Networks

Neural networks are computational algorithms inspired by the structure of the human brain. They consist of a layered structure of interconnected nodes. A node will receive inputs from the previous layer of nodes (or the input layer), multiple each input by the nodes weights and then pass the summation through an activation function as an output[22]. This process can be visualised in figure 3.3 (note, the activation function is f() in fig 3.3). The summation has a bias term which is essentially a constant that

is added to the summation of the weights and inputs. The activation function is most easily visualised by the relu function as seen in figure 3.2. When using the relu fucntion, if the input is less than 0 the output is zero, else the output is simply the input.

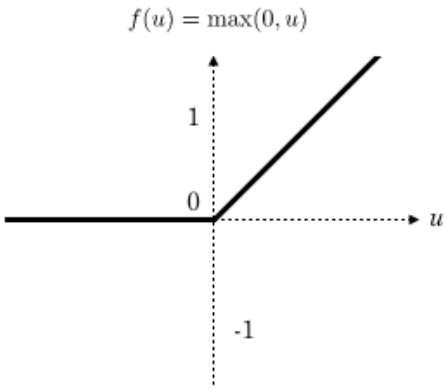


Figure 3.2: Relu activation function [23]

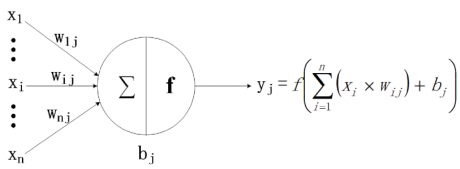


Figure 3.3: Representation of a node in a neural network[22].

During training the weights and basis of each node are gradually changed as it learns the mapping form input to output. The number of neurons per layer and the number of layers is entirely configurable, as is the number of connections between layers. This design forms the basis on many other networks.

### 3.1.4 Long Short Term Memory Networks

Long Short Term Memory (LSTM) networks are a type of Recurrent Neural Network (RNN) architecture that is particularly well suited for sequential data and time series analysis. Being a type of neural net they also include input layers, hidden layers with neurons, weights and biases and output layers. The special feature of an LSTM is that they are able to capture long-range dependencies. This is done by using a memory block that is in charge of remembering the neural nets' temporal state. A network of gates is used to control the flow of information through the memory block, namely input gates, output gates and forget gates. Input gates determine whether new information enters the cell. While f[24]

## 3.2 Data processing theory

In the context of machine learning, the preprocessing of data can play a major role in the algorithm's success.

Typically raw data has many different variables with different scales and units of measurement. This can lead to a model showing bias towards features with more extreme distribution values. While some machine learning algorithms are immune to these issues, they heavily affect the performance of others.

Feature scaling helps to solve this issue by transforming all of the data to a specific scale, distribution or range. Some of the most common methods include re-scaling, standardisation and normalisation. All of which can improve convergence speed and interpretability while decreasing risks such as overfitting.

### 3.2.1 Rescaling

Rescaling a vector is analogous to changing the units of measurement for the data. This is done by first adding or subtracting a constant and then multiplying or dividing by a constant.

An example would be data entries that hold units of energy that could be rescaled to be in the kilo-units (kW) from units (W).
Standardisation and normalisation are two common methods used to rescale data.

#### 3.2.1.1 Standardisation

The core aim of standardisation is to scale a set of data so that it fits a standard normal distribution. Meaning that after standardisation the data should have a mean of 0 and a standard deviation of 1. This process will change the values of the data set but keep the shape of the distribution the same. The formula is simple to apply, as seen in equation 3.3, where $\mu$ is the mean and $\sigma$ is the standard deviation.

$$\hat{X} = \frac{X - \mu}{\sigma} \tag{3.3}$$

However, it is important to note that the mean and standard deviation should be calculated on only the training data with the test data excluded. Once they have been calculated on the training data they can be applied to the test data set. This is to avoid the risk of data leakage.

For example:

Training Data: [1, 10, 3, 7, 5]
Test Data: [ 3, 6]
$\mu = \frac{1+10+3+7+5}{5} = 5.2$
$\sigma = \sqrt{\frac{(1-5.2)^2+(10-5.2)^2+(3-5.2)^2+(7-5.2)^2+(5-5.2)^2}{5}} = 3.124$

These values are then applied to both the training and test data according to the formula.
$\hat{X} = \frac{X-5.2}{3.124}$

#### 3.2.1.2 Normalisation

The main aim of normalisation is to fit data into a specific range, typically between 0 and 1. In a similar manner to standardisation, the process does not alter the shape of the distribution, in order to preserve information. The formula for normalisation is shown in equation 3.4.

$$\hat{X} = \frac{X - X_{min}}{X_{max} - X_{min}} \tag{3.4}$$

In a similar manner to standardisation, the values for $X_{min}$ and $X_{max}$ are calculated according to the training data and then applied to both the training and testing data.

## 3.3 Reinforcement learning theory

Reinforcement learning has several notable differences compared to other machine learning algorithms. In supervised learning methods, the data and the labelled target are fed into the training model in order

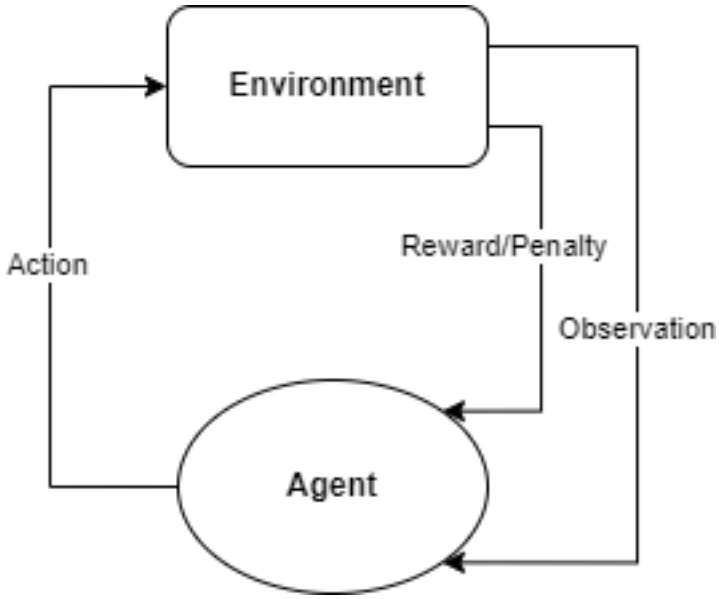


Figure 3.4: Simple visualisation of an agent interacting with an environment.

to learn some mapping. Where as in reinforcement learning the agent interacts with an environment and gathers its own data through an iterative process.

The core idea entails defining an environment for the agent to act in. The agent then makes an observation of the environment and can choose to make an action. The action is then applied to the environment. If it is a favourable action the agent can earn a reward, if it is not then it could be penalised. Such an interaction is visualised in figure 3.4. This interaction is repeated until the end of an episode. An episode can be ended by the agent reaching a goal(succeeding), meeting a termination requirement (failing), or reaching the maximum number of time-steps (truncated).

The agent will employ a policy during learning. This is essentially the strategy that the model will use to determine what its next action should be. Popular policies include Deep Deterministic Policy Gradients (DDPG), Proximal Policy Optimisation (PPO) and Soft Actor Critic (SAC) however, many other exist. Typically there are many hyperparameters that may need tuning in order to successfully train an agent.

The reward is an essential ingredient to training a successful model. If an action is rewarded to much it may lead to exploitation and the model will not reach the actual goal. If actions are too heavily penalised then the agent may choose to end the episode as quickly as possible to avoid incurring heavy costs. Rewards that are to sparse may result in a lack of quality data for the agent to learn from.

## 3.4 Machine Learning software

### 3.4.1 MATLAB

MATLAB offers an array of machine learning (ML) capabilities. Included in this are the Deep Network Designer, Classification Learner and the Experiment Manager apps. MATLAB has extensive documentation and a strong user base that will make the software easy to use and apply.

Due to its widespread use in the engineering field, this report will be making use of MATLAB by

MathWorks to perform the load forecasts.

#### 3.4.1.1 Python

Python is an incredibly popular language for machine learning. Due to its large user base it has a host of support and documentation.

Stable-baselines3 is a Python library written to facilitate reinforcement learning by providing a set of high-quality, easy-to-use and well documented implementations of RL algorithms. The library is designed to be user friendly and supports a wide range of RL algorithms, making it a valuable tool for researchers [25].

It includes popular algorithms such as PPO, DDPG, SAC and many more. A vital property is that it provides a platform to easily customise an environment, allowing a user to build and design their own.

Weights and biases is a machine learning experiment tracking platform. It offers a range of tools to log, visualise and analyse experiment metrics. It can easily be integrated into Python projects.

# Chapter 4

# Data collection and preprocessing

This section outlines the steps that were taken to collect and process the data. The implementation of the steps can be found in chapter 4.
From the literature review and from the project brief it was determined that in order to model a hybrid microgrid, data would be needed in the following key areas.

1. AC and DC load data
2. Time of use rates
3. Loadshedding occurrences

In order to ensure that the data was as relevant as possible, it was decided that a building on UCT upper campus would be used as a base for data collection wherever possible. In order to be able to work with hourly profiles all of the data needs to be in hourly intervals. The time frame that was decided on for data collection was the year of 2022.

## 4.1 AC and DC load data

The primary use of the load data is to train a model that is able to make accurate 24 hour forecasts. In addition to this, it will be used to size the hybrid microgrid and during the simulation of the energy management agent in the reinforcement learning environment.

Permission to use the load data from an academic building on UCT's upper campus will be requested. Once granted the buildings load profile will be used as the AC load. Due to the absence of available DC load it was decided that the DC load would have to come from an open source database. Ideally the open source data should come from an academic DC load profile.

Table 4.1 shows the headings of the data that was received from UCT. Columns that held identical values for every row were removed from the table immediately as they held no information.

The data from the UCT building was used to model the AC load for the hybrid microgrid. Unfortunately, the UCT building does not have a DC load. In order to model the DC component of the hybrid microgrid a data set with an hourly load profile was found in Mendeley data under a Creative Commons license [26]. A middle school's load profile was chosen as it showed restively similar trends and distributions to the UCT building data. The data was shifted to start on the same day of the year. Since it came from the northern hemisphere the data was shifted so that the winter season lined up with the winter in the southern hemisphere.

The AC load data from Menzies and the DC load data from Mendeley Data were joined into one table.

| Heading | Description |
|---|---|
| DC_load | The DC load profile was appended to the dataset |
| AC_load | UCT building system true power, in kilo-Watts (kW) |
| stot | UCT building apparent system power, in kilo-Volt-Ampere (kVA) |
| qtot | UCT building system reactive power, in kilo-Volt-Ampere Reactive (kVAr) |
| pftot | UCT building system power factor |
| md | UCT building maximum demand achieved |
| timestamp | Time and Date When the Data Point Was Measured |
| time | Time in 24 hour format |
| date | Date in yyyy/mm/dd format |
| day | Day of the week, eg. Monday, Tuesday ect. |
| tou | Time of Use eg. Off-peak, Standard, Peak |
| tou_id | Time of Use ID, a numerical representation of tou |
| week_number | Week number in the year. |

Table 4.1: Table headings for combined data

### 4.1.1 Cleaning load data

The data contained 6 rows with null entries. In order to preserve the time series characteristics as far as possible the values were not removed as this would create inconsistencies in the time steps. Instead, the previous value was used to fill the missing values.

While looking for outliers in the AC load it was clear to see that there were numerous instances of near-zero power being recorded as can be seen in figure 4.1. When the days that load shedding was implemented during 2022 were plotted over the Menzies electrical load plot, it was clear to see that these anomalies were due to load shedding. It was therefore necessary to replace all of these values since they would impede a model's ability to predict the load. The anomalies were cleaned by removing the lower 4.7 percentile of data and replacing the points using linear interpolation. The cleaning process is visualised in figure 4.2.

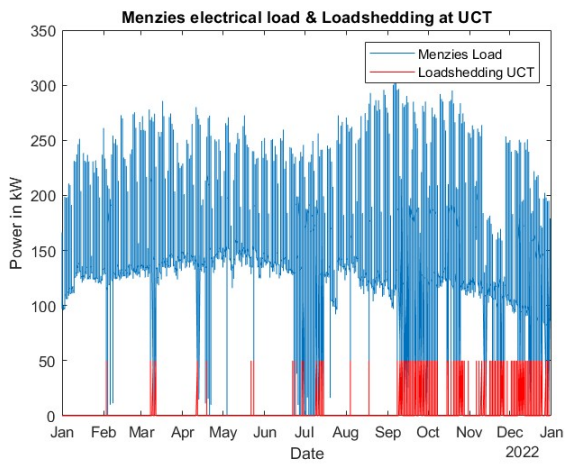


Figure 4.1: UCT building electrical load, overlayed with loadshedding at UCT.

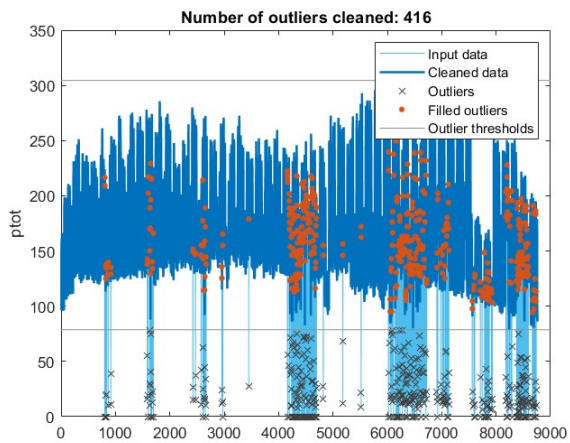


Figure 4.2: AC load and outlier replacement

The final AC and DC load data will be used in the design of the hybrid microgrid to size the generation

components. Furthermore it will be used to train a model to produce 24 hour load forecasts.

## 4.2 Time of use rates

Obtaining accurate Time of Use (TOU) rates is important as this is a key area that the agent is able to optimise. The agent needs to be able to learn that it is more expensive to purchase electricity during peak times and that it is cheaper to purchase during off-peak times.

The City of Cape Town's Rates tariffs were examined to extract the time of use rates for a large power user.

According to the city of the City of Cape Town's Annual Tariff Policies [1] An electricity tariff is defined based on the category of service provided. The categorisation of a user is based on the type of service, level of service consumption, type of connection, time of use and any other important factors.

The academic building will fall into commercial/industrial power user since it is not a lifeline or residential user. (CITE: Tariff Policies - 3 Categories of Users. 3.3). The max recorded power used was 300kW. Therefore, the academic building qualifies as a Large Power User with LV tariffs. (CITE: Chapter 5.2 Commercial/industrial)

The tariff structure that outlines the time of use tariff prices for the Large Power User with a Low voltage connection can be found in the city of Cape Town's electricity consumptive tariffs[2]. It is copied into table 4.3

| **Services** | **Unit** | **Remarks** | **R** (reg) | **R** (unreg) | **R** (total) | **R** incl. VAT |
|---|---|---|---|---|---|---|
| **High Demand** Jun-Aug | | Winter Months | | | | |
| Peak | c/kWh | | 483.99 | 31.42 | 515.41 | 592.72 |
| Standard | c/kWh | | 150.58 | 31.42 | 182.00 | 209.30 |
| Off Peak | c/kWh | | 84.39 | 31.42 | 115.81 | 133.18 |
| **Low Demand** Sept-May | | Summer Months | | | | |
| Peak | c/kWh | | 161.71 | 31.42 | 193.13 | 222.10 |
| Standard | c/kWh | | 113.10 | 31.42 | 144.52 | 166.20 |
| Off Peak | c/kWh | | 73.82 | 31.42 | 105.24 | 121.03 |
| Service Charge | R/day | | 133.69 | 0.00 | 133.69 | 153.74 |
| Demand Charge | R/kWh | | 219.93 | 0.00 | 219.93 | 252.92 |

Table 4.3: Time of use rates for a large power user in Cape Town

The city defines the periods for different time of use charges as follows.
Peak time of use: Weekdays 07:00 to 10:00; 18:00 to 20:00

[1] https://resource.capetown.gov.za/documentcentre/Documents/Financial%20documents/Annexure%207%20-%20Tariff%20Policies.pdf

[2] https://resource.capetown.gov.za/documentcentre/Documents/Financial%20documents/Electricity%20Consumptive%20Tariffs.pdf

Standard: Weekdays 06:00 to 07:00; 10:00 to 18:00; 20:00 to 22:00
Off Peak: All other times

This information was used to create an hourly data set with an associated TOU fee for the year. This data set was used in the design of the hybrid microgrid as an input to HOMER Pro. It was also used in the simulation of the Reinforcement Learning (RL) environment to calculate the cost of electricity in each timestep.

## 4.3 Loadshedding 2022 schedule

With South Africa's current energy crisis, loadshedding is a reality that might persist for years. Often polluting and expensive diesel generators are used to mitigate unmet load. It is vital that the agent learns how to manage loadshedding to reduce diesel usage and unmet demand.

Records of the loadshedding events that occurred at UCT were found through the City of Cape Town's records[27]. The raw dataset includes the loadshedding for all zones in the greater Cape Town area from the 2018 to September 2023. The events recorded for the year of 2022 in zone 15 were extracted as this is UCT's loadshedding zone. The resulting loadshedding events can be seen in figure 4.3, it is clear that load shedding increased drastically towards the end of the year. The distribution of loadshedding events according to the time of day can be seen in figure 4.4. The distribution curve shows that more loadshedding events happen during night hours compared to during the working hours.

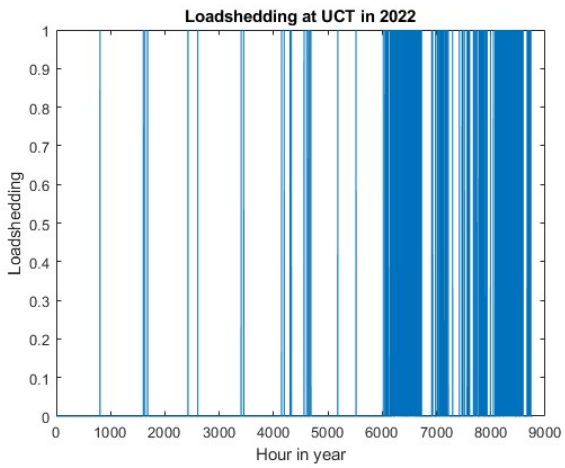


Figure 4.3

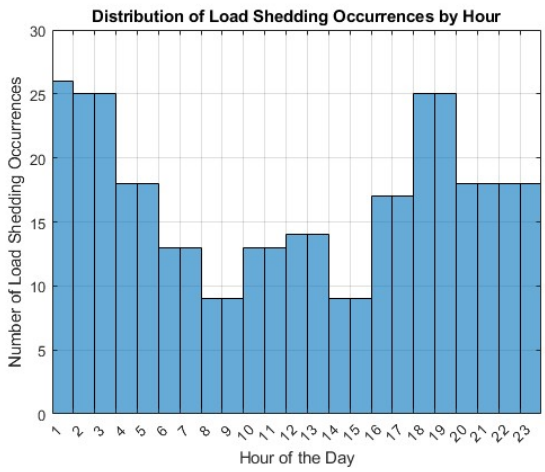


Figure 4.4

After the relevant data has been collected the load, TOU and loadshedding data will be used to design the hybrid microgrid. The load data will be used to train a model to make 24 hour load forecasts and finally all of the data will be used to train an autonomous energy management agent.

# Chapter 5

# Microgrid design

The design of the hybrid microgrid is a core aspect of the study as it dictates the environment in which the autonomous energy management agent will operate. The design should incorporate an AC and a DC load, ensure adequate generation to meet demand without excessive surplus generation, and remain economically feasible.

HOMER Pro is a powerful software tool that is widely used for the optimisation and design of microgrids in renewable energy ventures. It facilitates the modelling, simulation and analysis of energy systems, aiming to achieving optimal performance, cost-effectiveness and sustainability.

Users can fully configure inputs related to loads, energy resources, equipment specifications and economic parameters. HOMER Pro then executes an optimisation algorithm to find the configuration and sizing with the lowest Net Present Cost (NPC). To clarify NPC is the total cost incurred over the projects lifetime adjusted to a value in present time, accounting for both the discount rate and inflation.

In terms of component choices, wind turbines were selected to serve the AC load, while a PV array was chosen for the DC load. A lithium-ion battery bank will be used for the ESS. These selections stemmed from thier prevalent use in microgrids and the abundant availability of wind and solar power.

The sizing of the wind turbine, PV array, ESS and diesel generator will be accomplished with HOMER Pro, following this procedure:

1. Input data and parameters.
2. Evaluate proposed hybrid microgrids.
3. Adjust parameters if needed.
4. Finalise hybrid microgrid.

## 5.1 Design of Hybrid Microgrid

As can be seen in figure 5.2, the design will be a hybrid coupled AC microgrid, this descision was informed by the literature review.

The AC load along with wind turbines, a diesel generator and a connection to the utility grid make up the AC subgrid. The DC subgrid is made up of the DC load, a solar PV array and an ESS. A 2 way converter is used to transfer energy between the subgrids.

### 5.1.1 Homer PRO Input

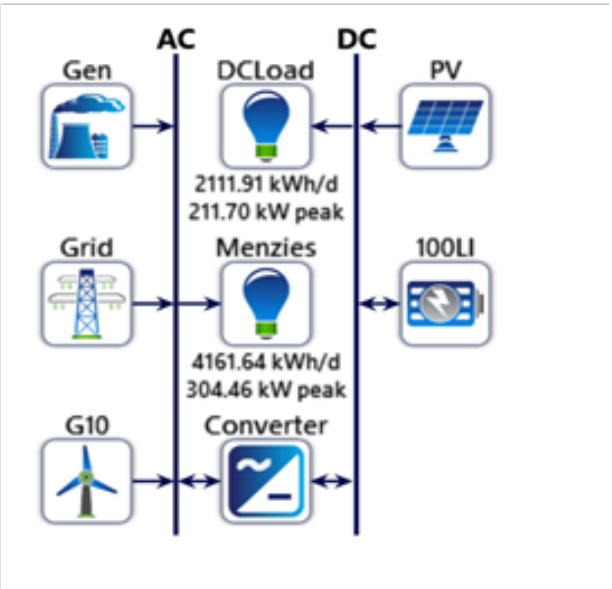


Figure 5.1: Input grid layout to Homer Pro.

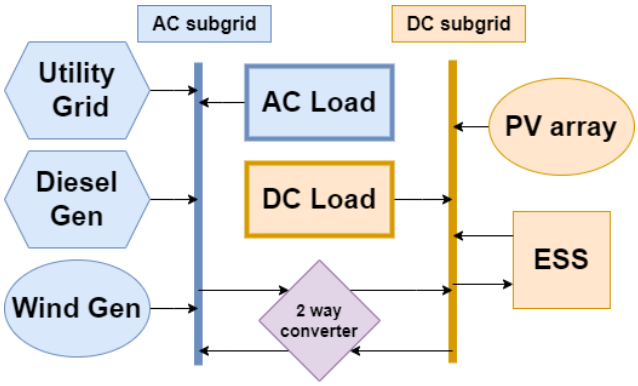


Figure 5.2: Input grid layout to Homer Pro.

#### 5.1.1.1 Load profiles

The data that was collected from UCT and cleaned in chapter 4 was used to model the AC load. The data collected from [26] in chapter 4 was used to model the DC load.

#### 5.1.1.2 Component pricing

Homer PRO requires pricing input for each component of the grid in order to find an economically viable solution.

In order to find rough approximations of the component prices, purchase prices were found online and averaged. A summary of the prices and final inputs is shown below in table 5.2. To find the references and purchases links please view the table in Appendix A, table A.2.

| Component | Size | Price (R) |
|---|---|---|
| Solar PV | 1 kW | 4 396.00 |
| Wind Turbine | 10kW | 48 598.00 |
| Diesel Generator | 1kW | 2 919.00 |
| Battery Li-ion | 100kWh | 646 963.00 |

Table 5.2: Input prices to Homer PRO

#### 5.1.1.3 Grid Reliability

In order to model the effects of loadshedding on the microgrid, the loadshedding schedule that was found in chapter 4 was used to set the grid outages in Homer Pro.

The aim being to see how loadshedding and an unstable grid would affect the sizing of microgrid components.

The economic penalty for a capacity shortage was set to R5/kWh. This was used to incentivise the optimiser to reduce unmet demand and find a system that was capable of meeting the load with an unreliable grid. It is important to note that the value of R5/kWh is not based off a real number as the monetary for unmet demand depends on the demand's use case. For example in a factory producing valuable products, unmet demand would have a large monetary cost associated with its. Since the building in question is an academic building there is no easy way to directly relate unmet demand to a monetary value. The final value of R5/kwh was set to be slightly higher than the cost of purchasing electricity to indicate to the optimiser that a capacity shortage is undesirable.

#### 5.1.1.4 Economic Factors

Inflation was set to a conservative 6% which is the estimated headline inflation for 2023 taken from a statement made by the South African Reserve bank [1]. It is worth noting that inflation of electricity prices has been much higher, however for simplicity the headline inflation was used.

#### 5.1.1.5 Sell in Tariff Structure

The city of Cape Town offers a feed-in Tariff. This is the price that it is willing to purchase energy from a non-residential small scale embedded generator. However, there is a condition applied that the user must purchase more energy than they sell to the grid.
It was decided that including the feed-in tariff would be excluded from this study in order to limit the scope of the project.

#### 5.1.1.6 Tariff Structure

The TOU rates that were collected in the chapter 4 were used to define the microgrid's tariff structure.

#### 5.1.1.7 Final grid input

The final input configuration to Homer PRO can be seen in figure 5.1. It includes an AC bus with the AC load, the grid, the wind turbines and a diesel generator. It also includes a DC grid with a the DC load, the PV panels, the Li-ion batteries and a 2 way converter.

### 5.1.2 Homer PRO output

HOMER Pro uses NPC to optimise microgrid sizing. The NPC represents the present value of the entire cost associated with a project over its lifespan, including initial investments, operational expenses, maintenance and potential replacement costs. It is used as the optimisation metric since economic feasibility is key to the success of any project.

Initially the simulation was run to find the overall NPC. However, the solution that HOMER Pro proposed was vastly oversized and impractical. As can be seen in table 5.3, the microgrid consists of 3.53MW generation capacity. This is far above the project brief of 1MW and the space required to install 1634 PV panels and 190 wind turbines would be extremely vast.

[1] https://www.resbank.co.za/en/home/publications/publication-detail-pages/statements/monetary-policy-statements/2023/Statement-of-the-Monetary-Policy-Committee-July-2023

| Component | Quantity | Specification | Total Capacity |
|---|---|---|---|
| Generic flat plate PV | 1634 | 1kW | 1634kW |
| Generic Wind turbine | 190 | 10kW | 1900kW |
| Diesel Generator | 0 | 0 | 0kw |
| Li-ion Battery | 0 | 100kWh | 0kWh |

Table 5.3: Component summary of HOMER Pro optimised system.

In addition to the system being impractical to install it also produces a huge amount of excess electricity. As shown in table 5.4, the grid produces 318% of the total load in excess electricity. While the grid has low NPC and a low unmet demand a more practical alternative would need to be found.

| Component | Energy (kWh/yr) | Percent total load |
|---|---|---|
| **Consumption summary.** | | |
| AC Primary Load | 1,512,922 | 66.3 |
| DC Primary Load | 767,845 | 33.7 |
| Total | 2,280,767 | 100 |
| **Production summary.** | | |
| Generic flat plate PV | 2,732,681 | 119.81 |
| Generic 10 kW | 6,435,644 | 282.17 |
| Grid Purchases | 387,226 | 16.98 |
| Total | 9,555,552 | 450.69 |
| **Excess and unmet load.** | | |
| Excess Electricity | 7,251,238 | 317.93 |
| Unmet Electric Load | 9,076 | 0.40 |

Table 5.4: Electrical summary of HOMER Pro optimised system.

It was decided that the maximum generation capacity of the Generic flat plate PV array would be limited to 500kw and similarly the generation capacity of the generic Wind turbine would be limited to 500kw. These limits were guided by the project brief which states that the microgrid should not have a capacity greater than 1MW. The HOMER Pro optimiser was run again to ensure feasibility. As expected the PV array and the wind turbines were set to their respective upper limits. However, the generator was sized to be huge at a max capacity of 560kW. This is grossly oversized and is only used to generate a total of 2 895kWh of power per year. In order to achieve more reasonable results, the generator was limited to 100kW capacity.

### 5.1.3 Final grid parameters

The composition of the final microgrid can be seen in table 5.5. It consists of a PV array with capacity 500kW, wind turbines with total capacity 500kW, a diesel generator with 100Kw capacity and a lithium-ion battery with 500kWh storage capacity.

In table 5.6 The amount of excess electricity has been significantly reduced to 42.8% of the total load while the unmet demand is reduced to nothing.

It is worth noting that according to HOMER Pro the NPC for running both loads entirely from the grid over a duration of 25 years is R3.16million while the NPC calculated for the final microgrid is

| Component | Quantity | Specification | Total Capacity |
|---|---|---|---|
| PV Units | 500 | 1kW | 500kW |
| Wind Units | 50 | 10kW | 500kW |
| Diesel generator | 1 | 100kW | 100kW |
| Li-Ion Battery | 6 | 100kWh | 500kWh |

Table 5.5: Component summary of 1MW generation capacity microgrid.

| Component | Energy (kWh/yr) | Percent of total load |
|---|---|---|
| **Consumption Summary.** | | |
| AC Primary Load | 1,518,997 | 66.3 |
| DC Primary Load | 770,836 | 33.7 |
| Total | 2,289,273 | 100 |
| **Production Summary** | | |
| Generic flat plate PV | 874,253 | 38.2 |
| Generic 10 kW | 1,693,591 | 73.97.0 |
| Diesel Generator | 2,607 | 0.11 |
| Grid Purchases | 731,780 | 31.96 |
| Total | 3,302,231 | 144.24 |
| **Excess and unmet load** | | |
| Excess Electricity | 980,269 | 42.82 |
| Unmet Electric Load | 9.78 | 0.00 |

Table 5.6: Electrical summary of final microgrid design.

almost a third of that at R1.35 million.

The final parameters of the hybrid microgrid will dictate the characteristics of the reinforcement learning environment used to train the energy management agent. Furthermore, they will be used to simulated the solar PV and wind turbine generation data.

## 5.2 PV and wind generation data

It is necessary to obtain an hourly dataset of the PV array and the wind turbines power generation. This dataset is needed in order to simulate the RL environment. Since the sizing of the PV array and the wind turbines is unique to the microgrid designed in this study, it was necessary to simulate generation data once the microgrid sizing was finalised.

### 5.2.1 Simulated generation data

Homer PRO was used to generate simulated PV and wind output with an hourly resolution with a window spanning one year. The PV system was a 500kW array and the simulated generation uses historical metodata that is extrapolated from satellite data. The wind system was comprised of 50 generic 10kW wind turbines.

The wind data can be found here: Simulated Wind Generation. The solar data can be found here: Simulated PV Generation.

A distribution of the energy generated according to the hour of the day is shown in figure 5.3 and 5.4

for the PV array and the wind turbines respectively.

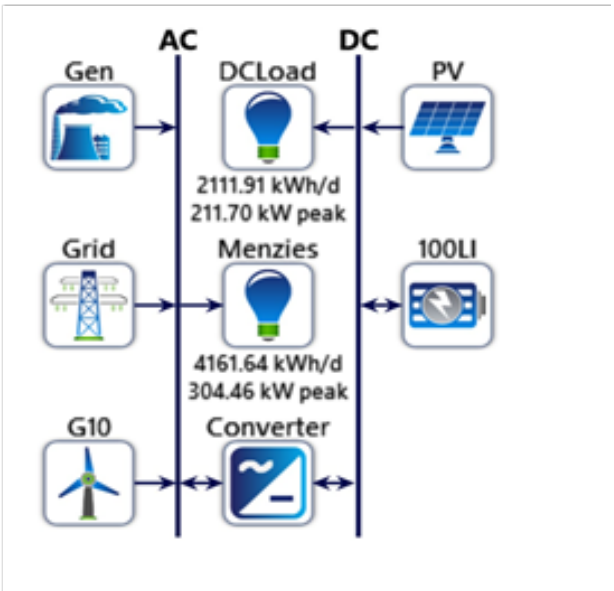


Figure 5.3: Distribution of energy generated by the PV array.

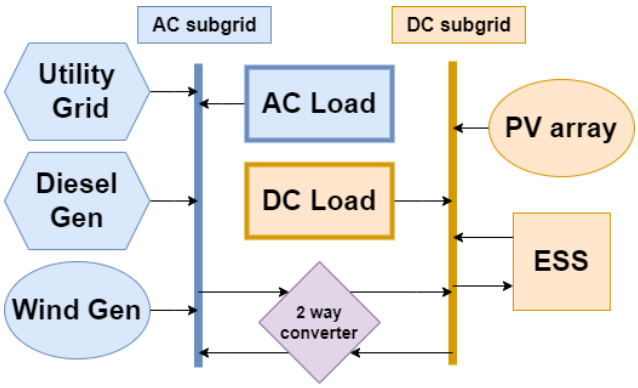


Figure 5.4: Distribution of energy generated by the wind turbines.

The simulated generation dataset was used to provide the RL environment with hourly generation values.

### 5.2.2 Generation forecasting note

A key section of energy management is to have a prediction of the generation capacity that a microgrid is going to have available at any point.

Sophisticated programs exist that provide this service, for example, solargis Forecast. However, these complete package programs can be expensive. It is also possible to use weather servies API's to retrieve forecasts of the necessary weather conditions. These forecasts can then be used to calculate an estimate of the generation capacity during the forecast window.

Given the existence of these sophisticated generation methods, it was deemed more practical to utilise them rather than undertaking the task of building a system from the ground up. This was an unfortunate but necessary descion that was made to keep the project within a reasonable scope. With more time it would be interesting to test the use of machine learning and historical data to make forecasts.

# Chapter 6

# Load forecasting

This chapter dives into training models that are able to perform timeseries forecasts. In the context of the study, it uses the load data that was collected in chapter 4 to train a machine learning model. The model will then be used in the energy management process by providing the agent with load forecasts for the next 24 timesteps.

The final models that were selected to be used for load forecasting were informed by the machine learning theory and the literature review. Three models were selected the LSTM, ARIMA, SARIMA and an ANN. The following steps were taken for each model:

1. Preprocess data into correct formats
2. Fit model parameters
3. Determine forecasting method

The machine learning theory regarding timeseries analysis is covered in Section 3.1.1. The theory behind each of these models is covered in subsection 3.1.4, 3.1.2 and 3.1.3 respectively.

The model that produces the best load forecasts will then be used in the final energy management system.

## 6.1 Exploratory Data Analysis

Code for this section can be found here. (Very rough and still a working version)

In order to further understand the data it is necessary to perform an exploratory data analysis. The aim is to unearth valuable insights, patterns and trends that may have initially been hidden. The focus will be on the load profile and consumption patterns in an attempt to inform our approach when using the data for predictions.

When observing a histogram of the distribution for the AC load data is distinctly bi-modal as can be seen in figure 6.1. This was expected and can largely be attributed to consumption during the day versus consumption during night.

However, what is interesting is that the AC load during the day also has two distinct peaks. This was further explored and it was determined that it arose from different usage patterns during working days and during weekend days. The breakdown goes further to show that weekends also have two distinct peaks, one for Saturday and another for Sunday as can be seen in figure 6.2.

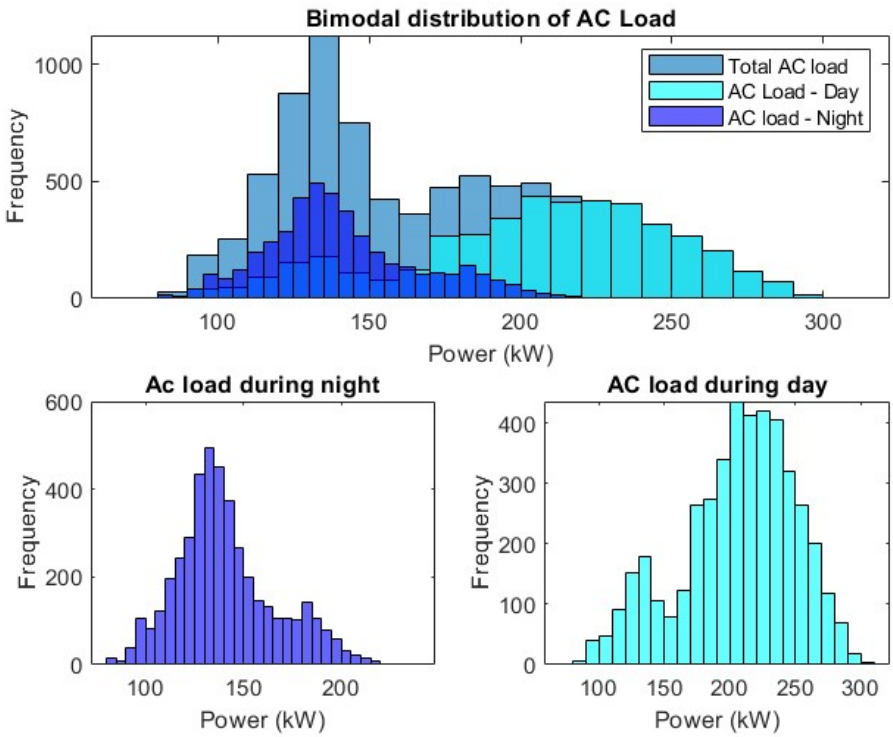


Figure 6.1: The bimodal distribution of the AC load.

The average hourly load profiles follow a very similar trend that is inline with what was expected. This can be seen in figure 6.5

The seasonality of the data can be seen through a boxplot of the average power used per month. There is a slight uptick in power usage during the winter months although it is not as prominent as was expected. The large number of outliers shown in the boxplots of the DC load was also unexpected. These outliers arise from the heavy skewness of the data with many more readings being taken outside of working hours and on weekends compared to at peak usage, leading to the median of the data being a comparatively low value.

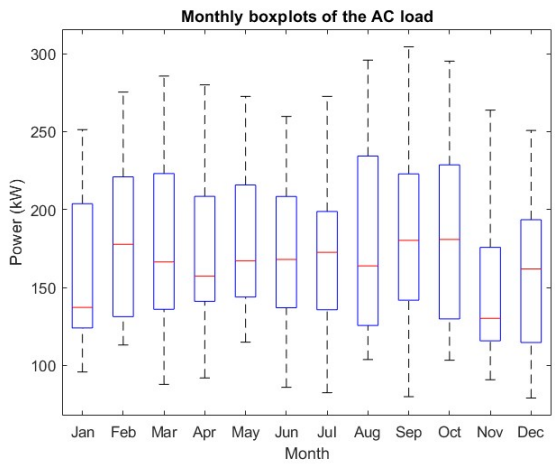


Figure 6.3: The average hourly AC & DC load profiles.

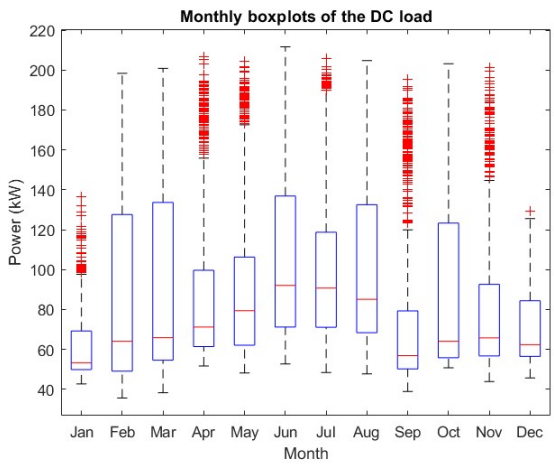


Figure 6.4: The average hourly AC & DC load profiles.

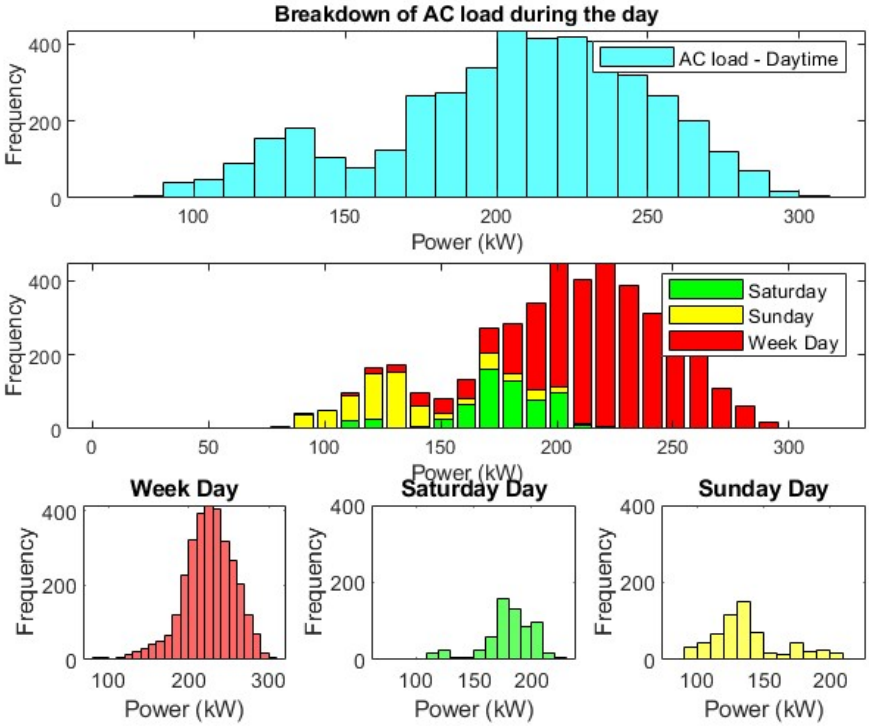


Figure 6.2: Breakdown of the AC load during the day.

### 6.1.1 Feature Selection

After the data was examined it was decided that indicator variables would be added to the table and tested. These were in the form of boolean values. An indicator was added for whether a reading was taken during working hours, on a weekday, or on a weekend. The header of the resulting dataset can be seen in table 6.1

Hot-one encoding is a technique used to convert categorical variables, such as the time of use id, into a format that can be provided to machine learning algorithms to improve predictions. The main reason that this can improve results is because machine learning algorithms assume that data has an ordinal relationship. This means that since the tou_id variable is defined as 1,2,3 to represent off-peak, standard, and peak times respectively, the model might assume that the peak category is equivalent to three times the off-peak category. This is not the case as they simply represent different times of the day.
For this reason, the tou_id was hot-one encoded. A new column was created for each category in the tou_id, each column now becomes that category and is 1 when the category is present in the original variable otherwise it is 0. The new off-peak, standard, and peak columns can be seen in table 6.1.
However, there are caveats to this approach. Hot-one encoding can rapidly increase the dimensionality of the dataset which can lead to increased computing cost and training time. Additionally, it can introduce collinearity which refers to a situation where two or more predictor variables in a regression model are highly correlated. Collinearity can lead to reduced generalisation and unstable training.

A heatmap of the correlation matrix for the data set can be seen in figure 6.6. This heatmap can give us an idea of which indicator variables that are known for a future timestep can be used to assist the

| tstamp | AC | tou_id | DC | weekDay | Sat | Sun | wrkHr | dayTime | Off-Peak | Peak | Standard |
|---|---|---|---|---|---|---|---|---|---|---|---|
| 01-Jan-2022 00:00:00 | 96.855 | 1 | 52.2 | 0 | 1 | 0 | 0 | 0 | 1 | 0 | 0 |
| 01-Jan-2022 01:00:00 | 97.053 | 1 | 52.0 | 0 | 1 | 0 | 0 | 0 | 1 | 0 | 0 |
| 01-Jan-2022 02:00:00 | 97.229 | 1 | 52.2 | 0 | 1 | 0 | 0 | 0 | 1 | 0 | 0 |
| 01-Jan-2022 03:00:00 | 96.859 | 1 | 52.2 | 0 | 1 | 0 | 0 | 0 | 1 | 0 | 0 |
| 01-Jan-2022 04:00:00 | 98.018 | 1 | 52.2 | 0 | 1 | 0 | 0 | 0 | 1 | 0 | 0 |

Table 6.1: Table containing potential features for machine learning.

model in predicting an unknown value. In this case the variables of interest are the AC and the DC columns. The heatmap shows that the AC variable has a strong positive correlation with the wrkHr indicator, to clarify wrkHr has a value of 1 during working hours and a value of 0 otherwise. It is interesting to note that the wrkHr indicator is a subset of the dayTime indicator that is able to hold more information about the AC variable.

The AC variable also has a strong correlation with the tou_id indicator as well as two of its hot-one encoded columns. The off-peak indicator has a strong negative correlation while the standard indicator has a strong positive correlation. The peak indicator seems to be much less correlated. In terms of collinearity the standard and the off-peak indicators have a strong negative correlation which could cause issues.

The DC variable has a similar set of correlation values to the AC variable, however, all of the indicators have slightly weaker correlations with the DC variable. This could be due to the DC values being simulated while the AC values are real measurements.

In summary, the wrkHr, Off-peak and Standard indicators have the potential to be useful indicators while attempting to predict the AC and DC variables however, the Off-peak and Standard indicators may introduce issues with collinearity. The tou_id may also be useful but might introduce a bias towards certain categories.

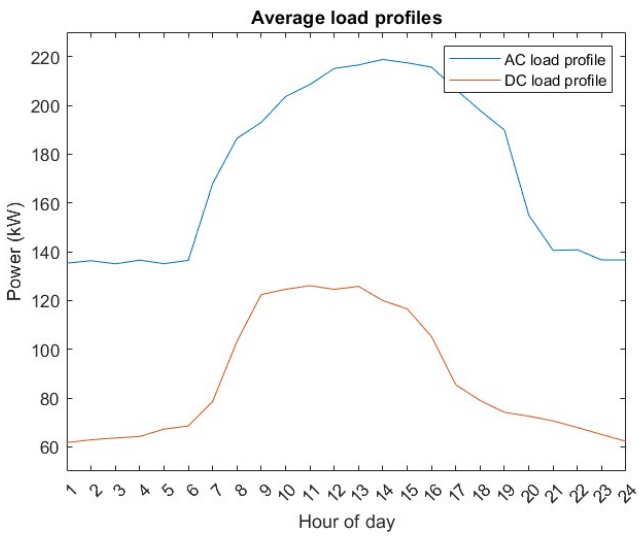


Figure 6.5: The average hourly AC & DC load profiles.

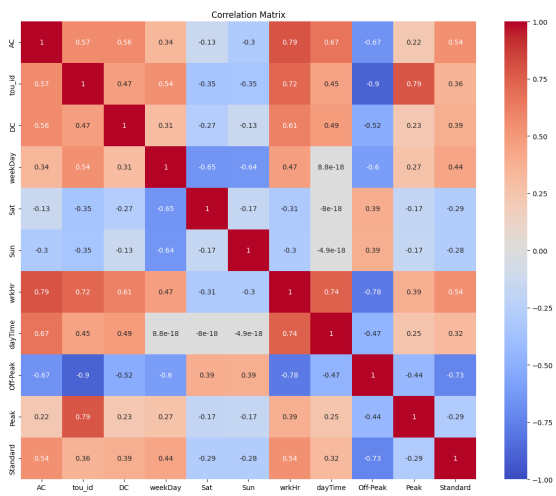


Figure 6.6: Heatmap of the correlation matrix.

## 6.2 Fitting LSTM model

In this step, we adapt the hourly electrical load data for LSTM, which excels at handling multivariate time-series forecasting. The data is first loaded and organised into a format that the model can use to train, it is then separated into a training and testing data set and normalised. The model is then trained and a forecasting method is developed to produce a 24-step-ahead forecast.

Code for this section can be found here. (Still needs to be organised...)

### 6.2.1 Data Preparation

The electrical load data that was prepared in the previous section was imported into the workspace. The data was re-organised from the imported table into a cell array. Since LSTM models are capable of multivariate predictions, multiple predictors can be used. The indicators that were found to have strong correlations with the load data were kept while all the other values were removed.

#### 6.2.1.1 Data Partitionig

The array was grouped into batches to improve training efficiency. The number of time steps in each batch should be enough to provide information about the time series but not so much as to slow the training down extensively. Different size batches were tested and it was found that a batch size between 14 and 35 days provided the best results.

The dataset is split into a 70-30 ratio for training and testing purposes, ensuring that the temporal sequence is preserved to maintain the time-series integrity. A target matrix is also created. To forecast the values of future time steps, the targets are specified as the training sequences with values shifted by one-time step. The training values are stored in the matrix XTrain and the training targets are stored in TTrain. The same idea is applied to the testing data with the test inputs being stored in XTest and the test targets being stored in TTest.

### 6.2.2 Normalisation

The mean and standard deviation for the training dataset were calculated. This was used to normalise, giving it a zero mean and unit standard deviation using the formula: $X_{normalised} = (X - mean)/sigma$ where $sigma$ denotes the standard deviation.
It is important to note that the testing partition was normalised using the mean and standard deviation calculated for the training data set. This code can be seen in figure 6.2.2.

```
    %Mean of training
meanX = mean(cat(2,XTrain{:}),2);
sigmaX = std(cat(2,XTrain{:}),0,2);
%Mean of training Targets
meanT = mean(cat(2,TTrain{:}),2);
sigmaT = std(cat(2,TTrain{:}),0,2);

%apply to the training data
```

```
for n = 1:numel(XTrain)
    XTrain{n} = (XTrain{n}-meanX)./sigmaX;
    TTrain{n} = (TTrain{n}-meanT)./sigmaT;
end
%apply to the test data
for n = 1:numel(XTest)
    XTest{n} = (XTest{n}-meanX)./sigmaX;
    TTest{n} = (TTest{n}-meanT)./sigmaT;
end
```

Listing 6.1: Code used to normalise data for LSTM training

The values for the mean and the standard deviation were stored so that the predictions could be transformed back into the original scale.

### 6.2.3 LSTM configuration and training

A basic LSTM configuration was first tested with an input layer, LSTM layer, fully connected layer, and a regression layer. The size of the input layer corresponds to the size of the input matrix. Both the number of LSTM layers and the number of nodes per layer are fully configurable. Typically more and larger layers are able to learn more complex relationships but take longer to train and may overfit the data. The final LSTM layer then feeds into the fully connected layer which feeds into the regression layer to estimate the next value. This can be see in listing 6.2.3
Different size LSTM layers were tested and it was found that the AC load was predicted best by a much smaller layer and that the DC load benefited greatly from having larger layers. The final configuration for the DC load LSTM model can be seen in 6.2.3

```
numChannels = size(dataCell{1},1);
layers = [
    sequenceInputLayer(numChannels)
    lstmLayer(128)
    lstmLayer(128)
    lstmLayer(128)
    fullyConnectedLayer(numChannels)
    regressionLayer];
```

Listing 6.2: LSTM configuration.

The ADAM optimiser was used to train the network due to its widespread popularity. The training converged around 2000 epochs with more training resulting in poor generalisation of the testing data. The left padding of the sequences was done to prevent the network from attempting to predict the empty values at the ends of inputs with different numbers of observations. These details can be seen in listing 6.2

```
    options = trainingOptions("adam", ...
```

```
    MaxEpochs=2000, ...
    SequencePaddingDirection="left", ...
    Plots="training-progress", ...
    Verbose=0);
```

Listing 6.3: LSTM training parameters.

### 6.2.4 Forecasting method

Closed loop forecasting is used to predict values **t** through to **t+k** when observations have been recorded for steps **1** through to **t-1**. The first step is to initialise the net to a set point. A prediction is then made for one step into the future. The net is then updated with the value of the prediction set to the current value. Another prediction is then made for the next step into the future (using the previous prediction value as the current value). This process is repeated for the number of time steps that are needed for the forecast. This is shown in listing 6.2.4

```
        net = resetState(net);
        offset =  j*timeStep+1;
        [net,Z] = predictAndUpdateState(net,X(:,1:offset-1));

        numPredictionTimeSteps = 24;
        Xt = Z(:,offset-1);
        Y = zeros(numChannels, numPredictionTimeSteps); % the 2 is for the 2 output channels

        for t = 1:numPredictionTimeSteps
            [net,Y(:,t)] = predictAndUpdateState(net,Xt);
            Xt = Y(:,t);
        end
```

Listing 6.4: Method used for closed-loop forecasting of LSTM model.

After all the predictions for a full 24 hours ahead have been made, values for all 24 timesteps are stored in an output array. The start point is then incremented by one timestep and another closed prediction for 24 hours is made. Using this method it is possible to make a 24-hour closed loop prediction starting from every timestep in the testing data. It is necessary to make lots of future predictions to be able to get an accurate estimate of the MAPE of the predictions.
An example of the output of what a day ahead forecast looks like can be seen in figure 6.7

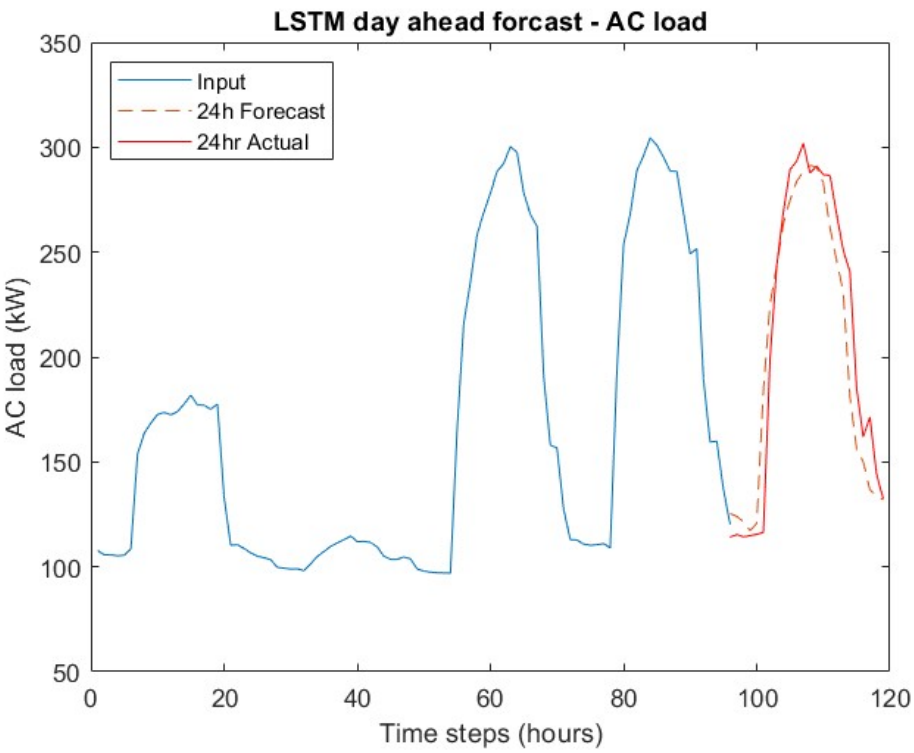


Figure 6.7: Day ahead forecast of the AC load using LSTM.

## 6.3 Fitting ARIMA model

Fitting an ARIMA model requires determining three key parameters for the model as covered in 3.1.2. These parameters are the auto-regressive order, p, the moving average order, q, and the differencing order, d. This section details the exploration of this process, the fitting of the model, and the final forecasting.
Code for this section can be found here. (needs to be organised, will move)

### 6.3.1 Data Preparation

An ARIMA model only accepts a single timeseries input, thus the data was streamlined to the core timeseries. That is a timestamp, the AC power, and the DC power.

### 6.3.2 Determining Model Parameters

**Determining the value of d:** The ACF of the data was examined and a Kwiatkowski–Phillips–Schmidt–Shin (KPSS) test was performed to determine if the data was stationary or not. The KPSS test returned that it was not stationary and the ACF showed that the series had many significant lags.

```
% KPSS test on AC and DC loads
[h_AC, ~, ~, ~] = kpsstest(data.AC, 'Alpha', 0.05);
[h_DC, ~, ~, ~] = kpsstest(data.DC, 'Alpha', 0.05);
```

Listing 6.5: KPSS test being used to test the data for whether it is stationary.

The data was then differenced and the same tests were repeated. The KPSS test returned that the data was stationary and the ACF looked much better. Although there were still some significant correlations as can be seen in figure 6.8. Additionally, there is a clear spike in the ACF around the 24th lag. This indicates that there is a solid seasonal component at the 24th lag. This is a good reason to attempt a SARIMA or SARIMAX model.

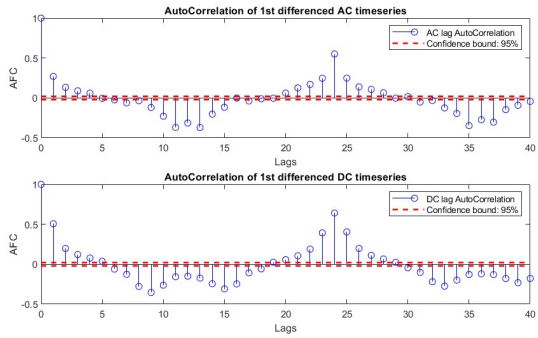


Figure 6.8: AFC of the 1st order differenced timeseries.

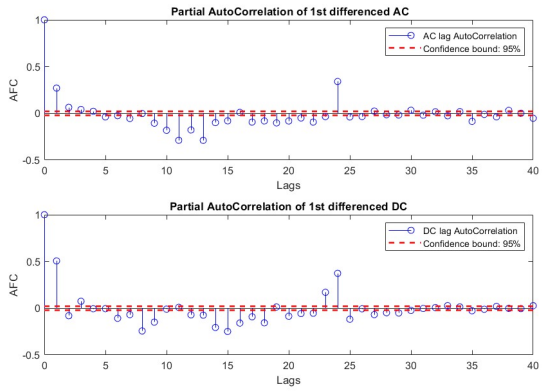


Figure 6.9: PAFC of the 1st order differenced timeseries.

A second differencing was attempted but the lag components quickly became highly negative. Therefore the simpler model with first-order differencing was selected for the initial tests.

**Determining the value of p:** In order to determine the value of 'p' the PACF of the first differenced sequence was taken as seen in figure 6.9. This showed that only 1 lag was significantly over the confidence bound in both the AC and the DC timeseries. The AC timeseries did have a 2nd and 3rd lag that were marginally over the confidence bound.

It was decided that a value of 2 would be used for p in initial tests.

**Determining the value of q:** The value of 'q' can be determined from the ACF of the first-order differenced series, shown in figure 6.8. Both the AC and DC series have 1 lag significantly over the confidence boundary. They also have 2-3 and 2-4 lags respectively that are marginally over the confidence boundary.

The value of q was first set to 2 to keep the model simple.

### 6.3.3 Training the model

The econometrics toolbox in MATLAB was used to try variations of the expected model inputs determined above. It was found that a model with p = 2, d = 1, and q = 2, produced the most accurate forecasts.

The code used to create and train the model is shown below in listing 6.3.3.

```
ARIMA_AC = arima('Constant',NaN,'ARLags',1:2,'D',1,'MALags',1:2,'Distribution','Gaussian');
ARIMA_AC = estimate(ARIMA_AC,X.AC,'Display','off');
```

Listing 6.6: Training of ARIMA model

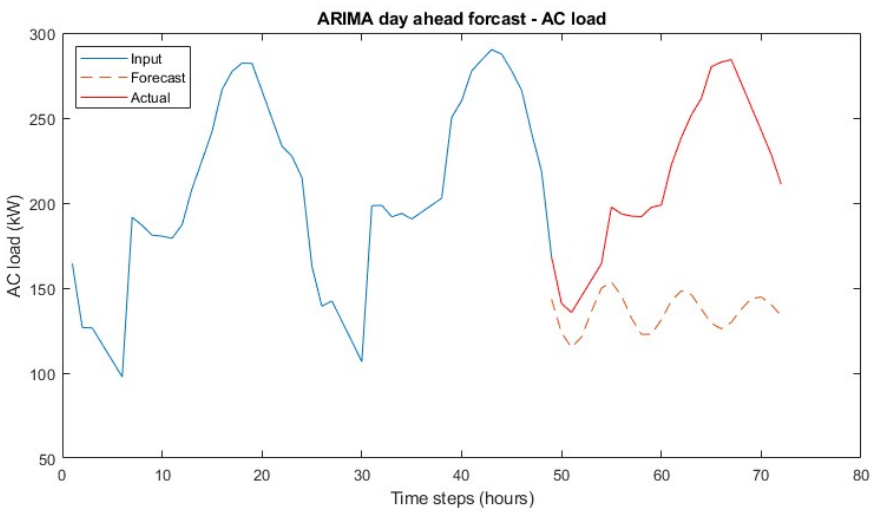


Figure 6.10: Day ahead forecast of the AC load using ARIMA model.

### 6.3.4 Forecasting method

ARIMA models in MATLAB have a built in closed loop forecast function. This was used to forecast 24 steps and produce day-ahead predictions of the load as can be seen in figure 6.10.
This did not prove to be a very accurate model and it was clear that the seasonal component of the series needed to be taken into account. It was therefore decided to fit a SARIMA network.

## 6.4 Fitting SARIMA model

Due to the strong sense of seasonality that appears in the ARIMA forecasting errors, it was decided that a seasonal model would be explored. Seasonal models have some additional parameters that need to be determined. Namely the seasonal auto-regressive component P, the seasonal moving average, Q, the seasonal differencing order, D, and lastly the seasonality which is the number of timesteps over which the seasonal pattern repeats.

### 6.4.1 Determining Parameters

In order to test the hypothesis that the time series needed to be seasonally differenced the first differenced time series was differenced at the 24 component as seen in listing 6.4.1. For example lets say that on day 1 at 8am the AC load was 230kw, and then on day 2 at 8am the AC load was 250kw. The seasonal difference refers to today's load minus yesterdays load so the seasonal differance value for day 2 at 8am is 20kw.

```
%First order differencing
ACdiff = array2table(diff(data.AC), "VariableNames","ACdiff");
DCdiff = array2table(diff(data.DC), "VariableNames","DCdiff");
data = [data(2:end,:) ACdiff DCdiff];

slag = 24; %seasonal lag component
%Seasonal differencing
```

| p values | d values | q values | P values | D values | Q values | S (seasonality) |
|---|---|---|---|---|---|---|
| [0, 1, 2] | [0, 1] | [0, 1, 2] | [0, 1] | [0, 1] | [0, 1] | 24 |

Table 6.2: SARIMA grid search parameters.

```
ACsdiffdiff = data.ACdiff(slag+1:end) - data.ACdiff(1:end-slag);
ACsdiffdiff = array2table(ACsdiffdiff, "VariableNames","ACsdiffdiff");
DCsdiffdiff = data.DCdiff(slag+1:end) - data.DCdiff(1:end-slag);
DCsdiffdiff = array2table(DCsdiffdiff, "VariableNames","DCsdiffdiff");
data = [data(25:end,:) ACsdiffdiff DCsdiffdiff];
```

Listing 6.7: Seasonal differencing of first order differenced timeseries.

After the timeseries were seasonally differenced the ACF was once again examined. The AC timeseries now displayed far less auto-correlation, with only one negative peak at the 24th lag. The DC timeseries still displayed a few significant lags however the overall image was much improved as can be seen in figure 6.11. To check that the DC timeseries did not need further differencing it was differenced again, however, the lags quickly went very negative and it was decided that no further differencing would be beneficial.

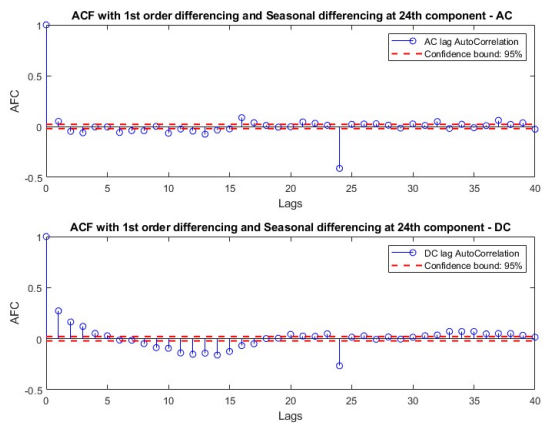


Figure 6.11: The ACF of the AC & DC timeseries with 1st order differencing and seasonal differencing at the 24th Component.

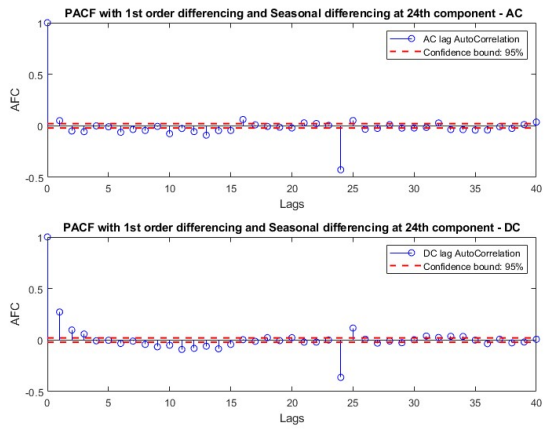


Figure 6.12: The PACF of the AC & DC timeseries with 1st order differencing and seasonal differencnig at the 24th Component.

The PACF was also plotted for the seasonally differenced timeseries, in figure 6.12. The plot for the AC timeseries showed no serious lags, indicating that the P value for the SARIMA model should be 0 or 1. The DC timeseries did however show some more significant lags indicating that some higher values of P should be tried.

### 6.4.2 Training Model

In order to find the best combination of input parameters. A grid search was performed across all of the parameters. The limits of the grid search were set using the information gathered from the ACF and the PACF plots. They can be seen in table 6.2. Grid searches are a common way to find the optimal parameters for ARIMA models and its variants.
The grid search iterativaly fits a model, validates the forecasts over a set of validation data and records the best parameters.

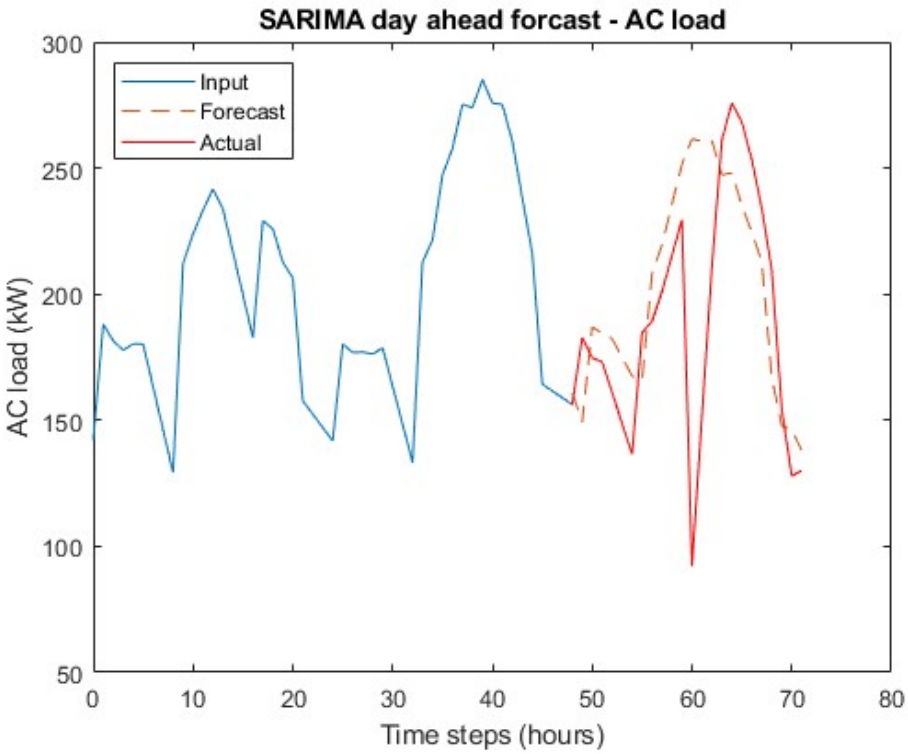


Figure 6.13: Day ahead forecast of the AC load using SARIMA model.

The best parameters that were found differed slightly from what was expected with values of (p=0,d=0,q=2)(P=1,D=0,Q=1)[24]. Most interestingly it was found that the model performed best without any differencing. This indicates that the data is more stationary than expected. The code used to create and train the model is shown below in listing 6.4.2.

```
SARIMA = arima('Constant',NaN,'D',0,'MALags',1:2,'Seasonality',24,'SARLags',24,'SMALags',24,
    ↪ 'Distribution','Gaussian');
SARIMA = estimate(SARIMA,X.load_data,'Display','off')
```

Listing 6.8: Training of SARIMA model

### 6.4.3 Forecasting method

Forecasting was performed in the same manner as for the ARIMA model. This time the results looked much more promising as can be seen in figure 6.13

## 6.5 Fitting ANN model

Code for this section can be found here. (Very rough and still a working version)

### 6.5.1 Data Preparation

For a basic regression model without any exogenous factors, the data was once again streamlined to just the core time series.

A 70/30 split was made with the training and testing data. To provide the model with targets an additional table was made with all of the observations shifted by one timestep.

### 6.5.2 Training Model

When training the model it was decided that a standard regression neural net would first be tested. The training options were defined as seen in listing 6.5.2, with a upper limit set on the number of training evaluations to prevent the model from over-fitting.

```
params = ...
opt = struct("ShowPlots",true,"MaxObjectiveEvaluations",100);
net = fitrnet(X_train, T_train,"OptimizeHyperparameters",params,"
    ↪ HyperparameterOptimizationOptions", opt);
```

Listing 6.9: Training parameters for regression net.

The 'OptimizeHyperparameters' function was set to optimise the parameters defined in 'params'. This was set to be the number of layers from 1 to 5, the layer weights initialisation, they layer biases initialisation and the size of each layer. The model was also set to to use standardisation and the relu activation function.

### 6.5.3 Forecasting method

In a similar manner to the closed loop forecasting that took place with the LSTM net it was necessary to write code that forecasted one timestep into the future, updated the model with that prediction and then used it to predict another timestep into the future. This method can be seen in listing 6.5.3.

```
    input = X_test(1:offset);
    first_forecast = predict(net, input);
    Yin = first_forecast(end:end);
    Y = zeros(24,1);
    Y(1) = Yin;

    for i=2:24
        input = [input(2:end)' Y(i-1)'];
        input = input';
        YNext = predict(net, input);
        Y(i)  = [YNext(end:end)];
    end
```

Listing 6.10: Forecasting with neural net.

The forecasting showed some promise but further investigation is needed. An example of what the day ahead forecast looks like can be seen in figure 6.14

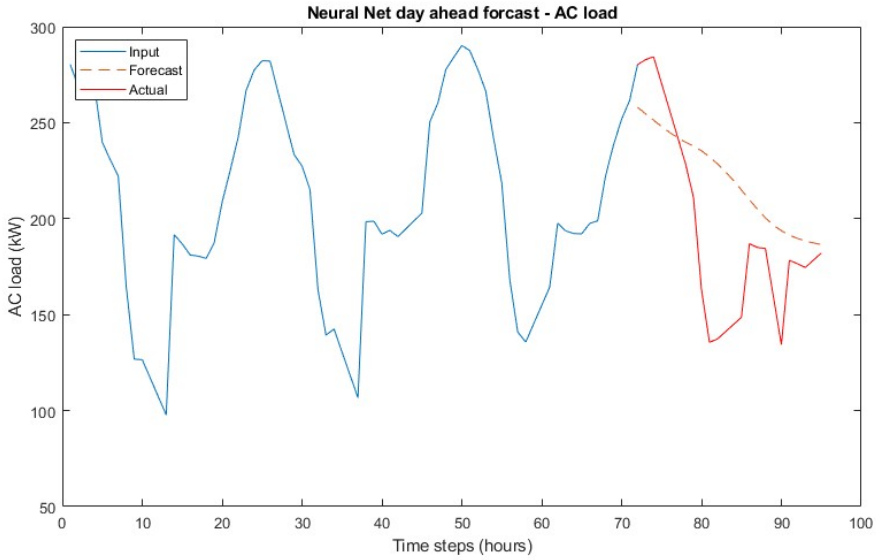


Figure 6.14: Day ahead forecast of the AC load using a regression neural net model.

# Chapter 7

# Load forecasting results and discussion

## 7.1 Results

In the realm of energy management, accurate 24-hour ahead forecasts are critical for performing energy scheduling. To identify the most suitable forecasting model, the three models that were trained in section 6 were evaluated based on their predictive performance.

### 7.1.1 Metrics of Evaluation

To compare the forecasting performance of the tested models, two primary metrics were employed.

- Root Mean Square Error (RMSE): Since this measures the average magnitude of the errors between predicted and observed values, it is a useful metric for gauging what the error is in the orginal units. For example, an RMSE of 43.2 would indicate that on average there is an error of 43.2 kW in the load forecast.
- MAPE: This provides a relative measure of the error in terms of a percentage, making it easier to interpret and compare across examples and scales.

It is expected that the accuracy of forecasts will drop further in the future as they progress. For this reason, the RMSE and MAPE were evaluated at every point in the forecast to observe the trend.

### 7.1.2 Forecasting Procedure

It was necessary to obtain many forecasts for each model in order to achieve an accurate idea of how the model performs. In order to do this the following steps were taken:

1. Make a 24-hour ahead forecast for the current timestep
2. Record the forecasted load values (all 24 values)
3. Store the actual values corresponding to those predictions (24 values)
4. Advance the timeseries by one step
5. Repeat steps 1-4 until a 24-hour-ahead forecast has been made for every value in the testing dataset.

The output is a cell array that stores the associated forecast and actual value for every timestep. This array can then be used to calculate the RMSE and MAPE.

When attempting to determine the mean MAPE and RMSE values over the 24-timestep window, an interesting challenge presented itself. Due to the large gradients present in some timesteps(typically morning and evening as power consumption changes rapidly), if the model predicts this change one timestep too early or too late, as illustrated in the figure 7.1 the corresponding timesteps absolute percentage error would be extremely large as can be seen at timestep 5 in figure 7.2. This large spike

will contribute heavily to the mean value of the MAPE and RMSE over the prediction period.

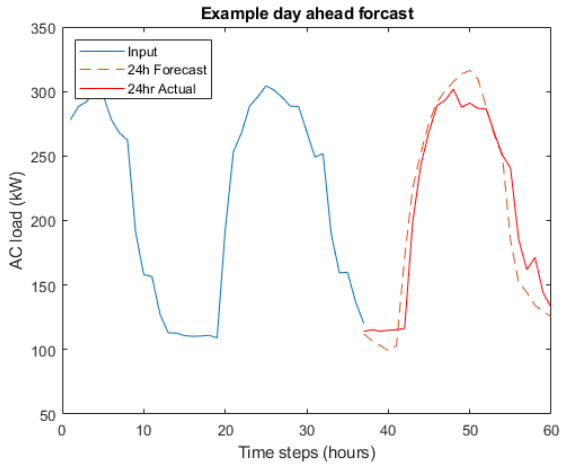


Figure 7.1: Example 24 hour ahead forecast

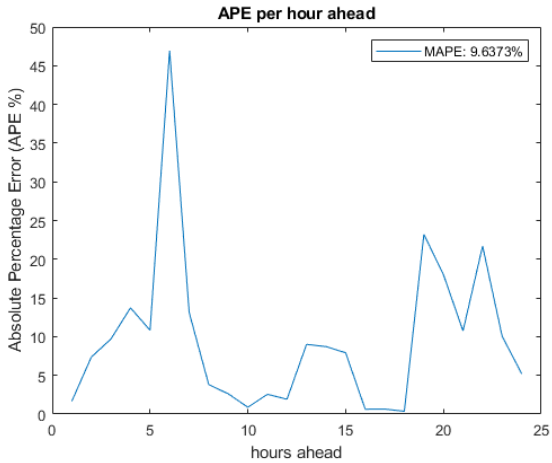


Figure 7.2: Large spike in error due to rapidly changing load.

While the per timestep error is a key indicator, it would also be useful to get a more accurate idea of what the total difference in power forecasts over the entire window. In order to do this the actual values and the predictions were both integrated over the forecast window, as seen in equation 7.1 and 7.2. While this gives a good indication of the total MAPE and RMSE for a given forecast, it could be misleading as values that have very different shapes but similar areas will return low errors. It would be ideal to use the difference between actual and predicted values, however in this case the discrete difference between the values is exactly what is causing the issue in the first place. In short, equation 7.1 and 7.2 can not be used alone but provide additional insight into the predictions.

$$total\ forecast\ MAPE = \frac{|\int_1^{24} Actual - \int_1^{24} Predictions|}{\int_1^{24} Actual} * 100 \tag{7.1}$$

$$total\ forecast\ RMSE = \sqrt{(mean\{[\int_1^{24} Actual - \int_1^{24} Predictions]^2\}} \tag{7.2}$$

### 7.1.3 Evaluation of the LSTM model

The MAPE for both loads can be seen in figure 7.3. For both loads the forecasts begin just below 10% MAPE at the first timestep, the gradient for the AC forecast flattens marginally around the 4th timestep while the DC load only flattens around the 10th timestep.

The RMSE is shown in figure 7.4. The RMSE for the AC load begins significantly higher than that of the DC load. However, once again the DC load's RMSE has a steeper gradient for around the first ten timesteps while the AC load has a change in gradient around the 4th timestep. The AC RMSE does not plateau quite as much as the DC RMSE.

The key metrics are summaries in table 7.1. The row 'Mean step' is simply the average value of all the per-step RMSE and MAPE values. The total column is the average over the forecasted window calculated using equations 7.1 and 7.2.

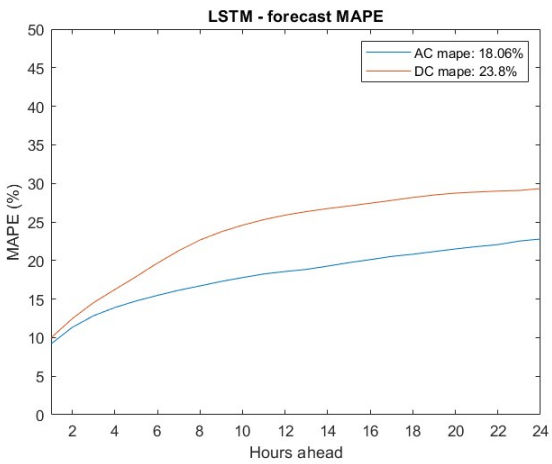


Figure 7.3: The MAPE per timestep of the day ahead LSTM forecasts

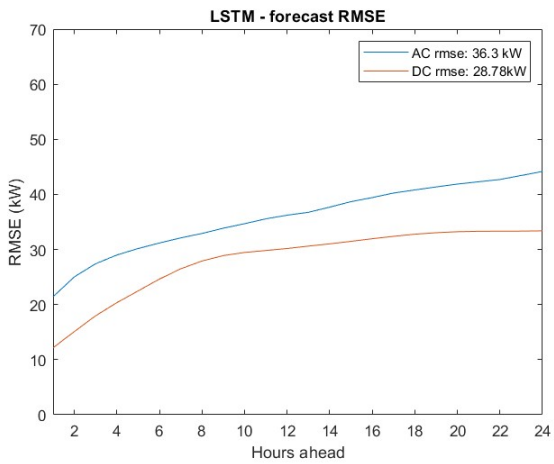


Figure 7.4: The RMSE per timestep of the day ahead LSTM forecasts

| | AC: **MAPE (%)** | DC: **MAPE (%)** | AC: **RMSE (kW)** | DC: **RMSE (kW)** |
|---|---|---|---|---|
| 1 step ahead | 9.18 | 9.97 | 21.42 | 12.15 |
| Mean | 18.06 | 23.80 | 36.30 | 28.78 |
| Total | 11.42 | 18.67 | 525.55 | 436.41 |

Table 7.1: Summary of results for the LSTM network.

### 7.1.4 Evaluation of the SARIMA model

The MAPE for both loads can be seen in figure 7.5. Both of the MAPE curves start relatively low, they sharply increase until timestep 4 after which they plateau.
The MAPE for the AC load is 8.74% while the MAPE per step is almost double at 16.82%. The MAPE calculated using equation 7.1 which represents the error in the area of the forecast compared to the area of the actual value is much lower than the mean per step error at around 11.05%. It is likely that this is a relatively good estimation of the error in the total amount of power forecasted since the SARIMA forecast matched the shape of the actual loads extremely well as can be seen in figure 6.13.
The DC load has slightly more error in the first time step at 10.27% and significantly higher mean per step error and total error with the total error being almost double the AC total error.
The RMSE is shown in figure 7.6. It follows a similar trend to the MAPE with a steep gradient in the first 4 timesteps and then a sudden plateau for the remaining forecasts. Since the RMSE is not scaled and the AC load has a higher mean than the DC load it makes sense that the AC RMSE will be higher than the DC rmse. Although it does make numerical comparisons between the graphs less valuable.

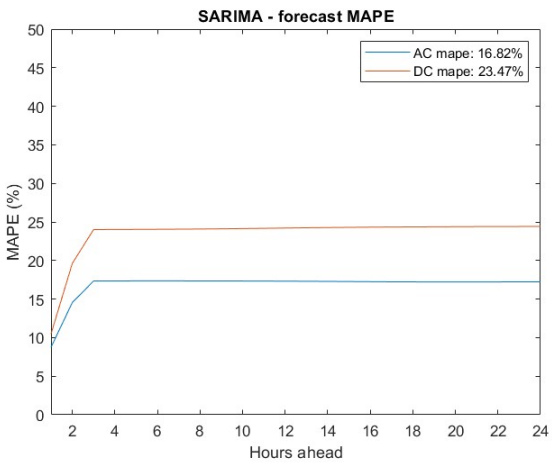


Figure 7.5: The MAPE per timestep of the day ahead SARIMA forecasts

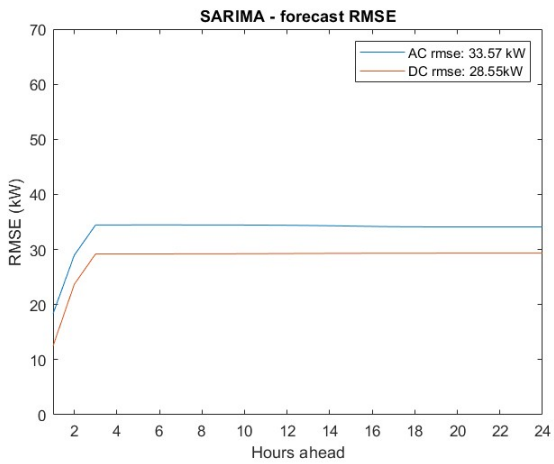


Figure 7.6: The RMSE per timestep of the day ahead SARIMA forecasts

| | AC: **MAPE (%)** | DC: **MAPE (%)** | AC: **RMSE (kW)** | DC: **RMSE (kW)** |
|---|---|---|---|---|
| 1 step ahead | 8.74 | 10.47 | 18.31 | 12.46 |
| Mean step | 16.82 | 23.47 | 33.57 | 28.55 |
| Total | 11.05 | 22.00 | 525.548 | 459.14 |

Table 7.2: Summary of results for the SARIMA network.

### 7.1.5 Evaluation of the Neural Net model

The MAPE of the neural net regression model can be seen in figure 7.7. The MAPE values for the first forecast ahead are low at around 7.5% for both the AC and the DC loads. The curves then have a similar shape as the error grows over the forecast horizon with a peak at 12 timesteps ahead. The errors then drop again towards the end of the forecast. The AC graph reaches its peak much lower than the DC graph at around 30% rather than 45%.

The RMSE of the neural net follows the same pattern and is shown in 7.8. Once again the AC load's RMSE is higher than the DC load's due to the difference in scale. The key metrics of both graphs are summarised in table 7.3.

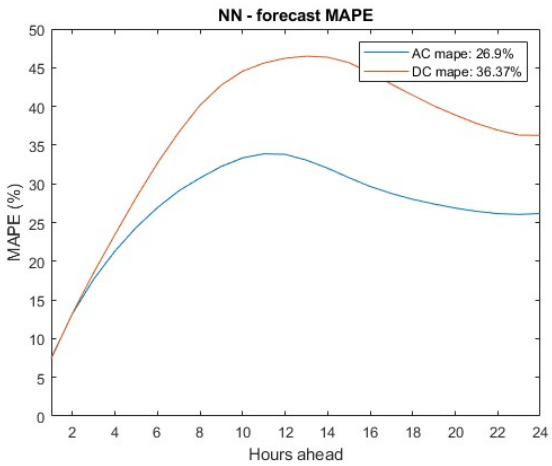


Figure 7.7: The MAPE per timestep of the day ahead NN forecasts

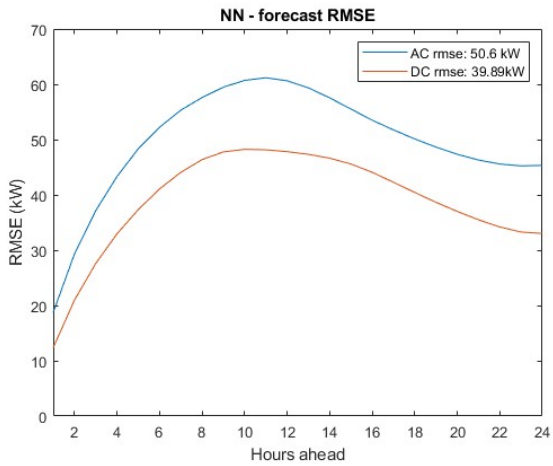


Figure 7.8: The RMSE per timestep of the day ahead NN forecasts

| | AC: **MAPE (%)** | DC: **MAPE (%)** | AC: **RMSE (kW)** | DC: **RMSE (kW)** |
|---|---|---|---|---|
| 1 hour ahead | 7.52 | 7.40 | 18.75 | 12.37 |
| Mean step | 26.90 | 36.37 | 50.60 | 39.89 |
| Total | 14.69 | 25.46 | 637.20 | 564.45 |

Table 7.3: Summary of results for the NN network.

## 7.2 Load forecasting Discussion

### 7.2.1 Model performance

The SARIMA model performed the best in all of the key metrics that were evaluated except for the 1st step ahead prediction. Additionally, the error in the forecasts was the most stable over the prediction window leading to the best overall results.
While the neural net was able to produce more accurate 1-step ahead predictions with 7.5% MAPE for both the AC and the DC load, both the mean step MAPE and the total MAPE were much higher than the other two models. It is interesting to see that while the neural net was extremely good at forecasting 1 step ahead it was not able to learn the seasonal pattern that occurs over the 24-hour daily load profile. This can be seen from how the errors are greatest at the 12-hour ahead step. Which is were the seasonal difference contributes the largest amount. The LSTM network was however able to learn this relationship far better, showing the power of the memory blocks incorporated in its structure. However, the SARIMA model, which is a more mathematical model, was able to account for the seasonal load profile the best after the correct parameters had been found. It was astounding how well the model was able to perform in the later timesteps.

### 7.2.2 AC and DC load variablity

Across all of the models the DC forecast performed far worse than the AC model, this prompted an investigation into the variability of both load profiles. Two common metrics in analysing load profiles are the day-to-day variability and the step-to-step variability. The day-to-day variability refers to the percentage that the mean daily power changes by. The step-to-step variability refers to how much the value will vary compared to its value in the previous time step. The day-to-day variability can be found by calculating the mean value for each day in the data set and then differencing the values to get the change from day to day. The standard deviation can then be calculated and turned into a percentage by dividing through by the mean of the dataset. The step-to-step variablity is calculated in a similar manner. The data is differenced once to find the change in each step. The standard deviation is then calculated and turned into a percentage by dividing by the mean of the data. The code used to do this can be seen in listing 7.2.2.

```
data = readtable("dataClean.csv") % read in data

step_diff = diff(data); %perfom stepwise differencing
step_std  = std(step_diff); % calculate the standard deviation per step
% caluclate step to step variability as a percentage
ac_step_var_pcnt = step_std.AC(1)/mean(data.AC(:)) *100
dc_step_var_pcnt = step_std.DC(1)/mean(data.DC(:)) *100
```

```

%calculate the mean power per day
data.dateOnly = dateshift(data.tstamp, 'start', 'day');
dailyMeans = groupsummary(data,'dateOnly', 'mean');

daily_diff = diff(dailyMeans); %perform differencing on the mean daily power
daily_std  = std(daily_diff);
%calculate the day to day variability as a percentage
ac_daily_var_pcnt = daily_std.mean_AC(1)/mean(dailyMeans.mean_AC(:)) *100
dc_daily_var_pcnt = daily_std.mean_DC(1)/mean(dailyMeans.mean_DC(:)) *100
```

Listing 7.1: Code used to calculate the variability in the loads.

The results of this operation can be seen in table 7.4. It can clearly be seen that the DC load has a much higher variability in both measures. This explains why the models were consistently performing worse when attempting to forecast the DC load. The comparatively lower step-to-step variability compared to the day-to-day variability also explains why the models without a built-in understanding of the seasonal pattern such as the regression neural net were able to rather accurately predict one step ahead but were not able to predict the rest of the days load without incurring huge errors.

| Load | Step to step variability (%) | Day to day variability (%) |
|---|---|---|
| AC load | 10.536 | 14.7 |
| DC load | 15.21 | 30.017 |

Table 7.4: Step-to-step and day-to-day variability of the loads.

### 7.2.3 Final load forecasting model

Due to its low mean step and total MAPE values the SARIMA model was chosen as the best model. Additionally, the SARIMA model has comparatively fast compute times compared to the LSTM and the Neural Net models making it better suited to being integrated into a larger model.

# Chapter 8

# Energy management agent

This chapter delves into the application of RL to create an autonomous energy management system. Building upong the hybrid microgrid that was designed in chapter 5, the microgird is transformed into an RL simulation environment. This simulated microgrid is then run over a span of a year, with hourly timesteps, employing the data accumulated as described in chapter 4. A crucial aspect of this system is the agent's access to load forecasts, which have been previously established in chapter 6. Before delving into the actual implementation, we will briefly discuss the application of RL theory to the energy management problem, setting the stage for the subsequent steps.

**Implementation of reinforcement learning**

The implementation process evolved iteratively, with each iteration adding complexity to the RL simulation. Initially, the environment featured a singular load, one source of generation, and basic TOU rates. As updates were rolled out, new features were introduced, such as loadshedding, two loads, and two forms of generation. The final layer of complexity was added with the integration of a demand charge.

1. Initiate with a basic environment.
2. Train the agent.
3. Test the agent's performance.
4. Enhance the environment by adding a new feature.
5. Repeat steps 2-4, refining until the desired environment complexity was achieved.

## 8.1 Reinforcement learning applied to EMS

Building upon the discussion in the reinforcement learning theory section **??**, it is clear that RL offers a potent tool for training agents to navigate complex environments. In the context of this study, the agent represents the EMS, while the microgrid serves as the environment. Through iterative training, the agent should learn to master energy management, aiming to reduce penalties for inefficient actions. A visualisation of this application can be seen in figure 8.1.

The environment's configuration aligns closely with the parameters delineated in the hybrid microgrid design section, with some simplification such as ignoring electrical lossess. This encompasses the AC and DC loads, the PV array, wind turbines, the battery system, and the converters.

For the agent to make informed actions, it is furnished with current and forecasted observations from the environment. Immediate data would include current loads, generation metrics, and battery levels. Meanwhile, predictive observations comprise load forecasts, generation forecasts, upcoming energy pricing, and the loadshedding schedule.

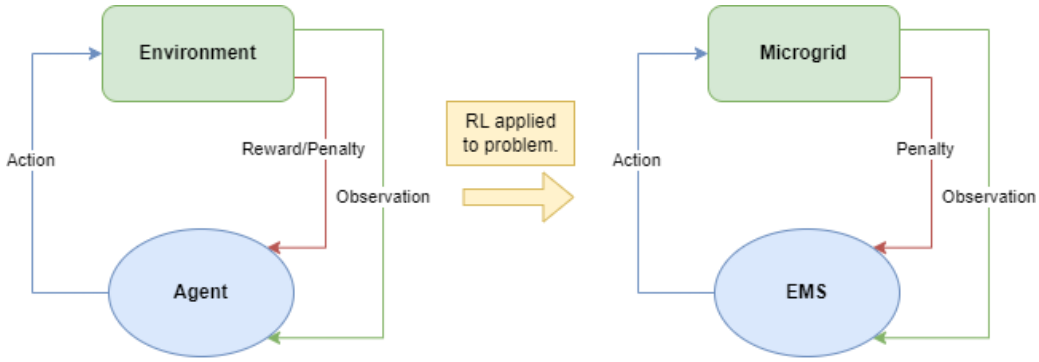


Figure 8.1: RL applied to the challenge of energy management.

## 8.2 Simplified environment

To clarify the development of the RL approach there are some key terms used in the stable-baselines3 library that should be elaborated on.

The 'environment' is the term that refers to the class that initialises the space that the agent will explore and learn to navigate. It also defines key functions that are used to simulate the behavior of the environment and facilitate interaction between the agent and the environment. The required set of functions for a custom environment to integrate with the stable-baselines environment can be seen in listing 8.2.

A brief summary of them is as follows:

- **Observation space**: Represents the data that the agent receives about the environment. This is used for the agent to make a decision on its course of action.
- **Action space**: This defines the set of actions that the agent can take.
- **Step function**: Invoked after the agent selects an action. It administers the selected action, updates the environment, and updates the agent's observation space accordingly.
- **Reset** This function resets the environment and readies it for a fresh training iteration or an evaluation run.

Other standard functions that can be integrated into the library include the render and the close function, neither of which were necessary for this project.

```
class CustomEnv(gym.Env):
    """Custom Environment that follows gym interface."""
    metadata = {"render_modes": ["human"], "render_fps": 30}
    def __init__(self, arg1, arg2, ...):
    super().__init__()
    # Define action and observation space
    #Example action space
    self.action_space = spaces.Discrete(N_DISCRETE_ACTIONS)
    #Example for observation space
    self.observation_space = spaces.Box(low=0, high=255, shape=(N_CHANNELS, HEIGHT, WIDTH),
    ↪ dtype=np.uint8)

    def step(self, action):
```

```
    ...#Define a step function
    return observation, reward, terminated, truncated, info

    def reset(self, seed=None, options=None):
    ...#Define a rest function
    return observation, info

    def render(self):
    ...#Optional
    def close(self)
    ...#Optional
```

Listing 8.1: Class definition of a custom environment in stable-baselines3.

The upcoming subsections detail the step-by-step process that was followed to develop a simplified environment in alignment with the guidelines provided by the stable-baselines3 documentation.

### 8.2.1 Environment

While drafting the initial version, the emphasis was on simplicity while retaining the fundamental attributes of a microgrid and the EMS
to streamline the design:

- Only one load was incorporated, opting for the AC load data, while the DC load was omitted.
- In terms of generation, only the output from the PV array was factored in, ignoring the contributions from the wind turbines.
- System intricacies, such as converter losses, loadshedding, and demand charges were set aside.

The primary objective for this rudimentary EMS agent revolves around proving its ability to reduce energy costs incurred by grid purchases. It serves as a proof of concept, showing the agent's potential to recognise the financial advantages of purchasing and storing energy during off-peak times to avoid peak prices.
These simplifications paved the way for an initial test environment, providing a preliminary benchmark. Below is an outline detailing the steps undertaken to establish the environment. For an in-depth exploration, the complete code can be accessed here.

#### 8.2.1.1 Observation space

The observation space defines the information that the agent can perceive about its environment. It can be imagined as the agent's eyes into the world that it exists in.
The initial observation space was defined with the code seen in listing 8.2.1.1. The space is defined in a dictionary format (Dict), where each entry has a key and an associated expected value range, shape, and data type.
For example, in the first entry 'load_forecast' is the key, and 'gym.spaces.Box(low=0, high=np.inf, shape=(1,num_preds), dtype = np.float)' indicates that it is expecting a 1D array that is 'n_preds' long where every value in the array is expected to be a floating point number equal to or between 0 and positive infinity.

```
# Dict space to store all the different types of observation
self.observation_space = spaces.Dict({
    "load_forecast": gym.spaces.Box(low=0, high=np.inf, shape=(1,num_preds), dtype=np.float32),
    "gen_forecast": gym.spaces.Box(low=0, high=np.inf, shape=(1,num_preds), dtype=np.float32),
    "price_forecast": gym.spaces.Box(low=0, high=np.inf, shape=(1,num_preds+1), dtype=np.float32),
    "bat_level": gym.spaces.Box(low=0, high=np.inf, shape=(1,), dtype=np.float32),
    "current_load": gym.spaces.Box(low=0, high=np.inf, shape=(1,), dtype=np.float32),
    "current_gen": gym.spaces.Box(low=0, high=np.inf, shape=(1,), dtype=np.float32),
    })
```

Listing 8.2: Observation space of simplest working version.

It's crucial to emphasize that in these initial versions, the load forecasts are not based on predictive models. Instead, they directly use the upcoming 24 actual values for the load and generation, giving the model perfect foresight in this phase. Furthermore, while a key is named 'price_forecast', it doesn't currently provide the monetary value of energy cost. It instead offers the time-of-use ID corresponding to each hour, distinguishing between off-peak, standard, and peak periods.

#### 8.2.1.2 Action space

The action space defines the actions that the agent can take within the environment. In this initial version, two actions are available to the agent: **standby** or to **fully charge its batteries**.

**Standby:** Opting for the standby action allows the agent to rely on a pre-established, rule-based system to manage the grid. This is a brief summary of how the standby action unfolds:

- Renewable generation attempts to meet the load demand.
- Excess generation is used to charge the battery.
- Shortfalls in generation draw on the battery's charge.
- If the battery level falls below its minimum threshold, the remaining shortfall is purchased from the grid.

To avoid confusion, the agent is **not** tasked with orchestrating the process listed above. By choosing the standby action, the agent merely signals the microgrid environment to implement this set of predetermined rules. Refer to figure B.1 in Appendix B for a visual breakdown of the final implementation of this set of rules.

**Fully charge batteries:** This action is designed to be used if the agent forecasts impending power shortages during peak times and allows it to preemptively purchase and store electricity during off-peak times. When this action is chosen:

- The total energy requirement is calculated as the sum of the immediate load demand and the energy necessary to fully charge the battery.

- The net energy to be purchased from the grid is calculated by subtracting the current renewable generation from the total energy requirement.

As a result, the battery will always be recharged to its full capacity after this action has been selected. Note that loadshedding is not present in the environment at this stage so the grid can be assumed to always be available.

#### 8.2.1.3 Reward

The design of the reward function serves to encourage the agent to minimize energy purchase costs. Specifically, the reward for an action is computed as the product of the energy purchased from the grid during that step and the corresponding TOU multiplier. As mentioned the TOU rates at this stage did not relate to a monetary value but were designated as follows:

- Off-peak = 1
- Standard = 2
- Peak = 3

To reflect the objective of minimising energy costs, the reward is negated (multiplied by -1). Thus, in the context of the agent's learning, it is perceived as a penalty to be minimised rather than a reward to be maximised.

#### 8.2.1.4 Step function

Each step progresses the agent one time step through the environment (one hour). After an agent chooses an action, the action is applied to the current step. The new observation state is calculated along with the reward function. Both are then fed back to the agent for it to decide on its next action. The step function is a core mechanism within the RL framework. Every time it is invoked, it advances the agent by one time unit in the environment, which in this context, equates to one hour.

- It implements the 'standby' or 'fully charge battery' function depending on the agents selection.
- The new observation for the agent is determined
- Concurrently, the reward for the selected action is calculated.
- The new observation space and the reward are relayed back to the agent for it to select its next action.

### 8.2.2 Results of EMSv0.1

This initial version, despite its simplicity, yielded promising outcomes. For training, 70% of the available data was allocated to the environment. The agent was trained using various algorithms, such as the Proximal Policy Optimiser and the Actor Agent Critic, over 1.5 million timesteps.

Subsequently, the agent was tested in a separate environment, utilizing the remaining 30% of the dataset. To establish a baseline, a reward was computed by simulating an entire episode of the environment in standby mode. This baseline reward approximates the agent's performance if it opted solely to purchase energy needed with no planning.

A simulation was then run with the trained agent making decisions. The agent showcased its ability to enhance its reward, effectively reducing the penalty associated with energy costs by 8%. Although,

this improvement cannot be equated to monetary savings in this phase, it undeniably indicates the agent's proficiency in making preemptive electricity purchases, thereby avoiding peak prices at a later timestep.

This promising behavior is evident upon reviewing figure 8.3 In this figure, the green bars represent the trained agent's data, while the red bars indicate the higher penalties incurred without the agent. Notably, the agent has reduced penalties during both standard and peak times, while increasing the energy during off-peak times. Consequently, the agent has successfully achieved a reduced overall penalty.

Figure 8.2: Reward accumulated without an agent vs with a trained agent.

Figure 8.3: The penalty incurred by the agent per time of use category.

## 8.3 Development of the Environment and Agent

The development of the RL microgrid environment followed an iterative approach. With each iteration, the system was tested against a base case to confirm its ability to energy cost savings. While it's beyond the scope of this section to delve into the details of every iteration, a comprehensive summary of additions and changes can be found in table B.2 in Appendix B.
Several milestones punctuated the development journey. These include the incorporation of loadshedding, the handling of both AC and DC loads, and generation - central to the hybrid nature of the microgrid as envisioned in the project scope. Subsequently, tangible monetary costs were introduced, followed by the integration of a demand charge.

### 8.3.1 Implementation of a hybrid grid and load shedding

This version incorporated the AC & DC loads, Wind & PV generation, and UCT's 2022 loadshedding schedule. A diesel generator, limited to 100kw, was introduced in accordance with the hybrid microgrid design. The rule-based structure was adjusted to account for these changes. Most notably if there is an energy shortage and the utility grid is unavailable, the generator activates. Any additional shortage is recorded as unmet load. Details of the final rule scheme are in Appendix B, figure B.1. The reward function was also updated to include a penalty for unmet demand and the cost of diesel generation.

The agent adapted well to this environment, surpassing baseline rewards as can be seen in figure 8.4 and 8.5. The agent is able to reduce operating costs by 10%.

The monetary cost comprises energy purchase costs and diesel generator expenses, calculated at 0.4l of diesel per 1kWh (diesel priced at 23 rand). Refer to figures 8.4 and 8.5 and listing 8.3.1 for more details. While the reward is calculated as the monetary cost with an additional term to penalise the unmet load as mentioned earlier.

```
# 0.4l per kWh produced multiplied by a cost of 23 rands per litre.
diesel_cost =self.diesel_gen[self.current_step]* 0.4*23
#Amount of electricity purchased multiplied by the cost of electricity for that step.
elec_purchase = self.step_purchased[self.current_step]*self.purchase_price[self.current_step]
#money spent in that step is the sum of the two values.
self.money_spent[self.current_step] =  elec_purchase +  diesel_cost
```

Listing 8.3: Calculation of monetary cost.

Figure 8.4: Reward accumulated without an agent vs with a trained agent in environment v1.2.

Figure 8.5: Total cost incurred by the agent per time of use category in environment v1.2.

With the implementation of loadshedding, the agent proactively purchases more energy in anticipation of grid unavailability. Although this increases the total energy purchases, savings in the resulting reduction of diesel generator use offset this. Notably, the agent's strategy results in a 75% reduction in unmet load, which is substantial. Figure 8.6 visualises the increase in energy purchases across the TOU rates, and Figure 8.7 illustrates the large reduction in generator usage and unmet demand.

Figure 8.6: The cost of purchases by the agent per time of use category in environment v1.2.

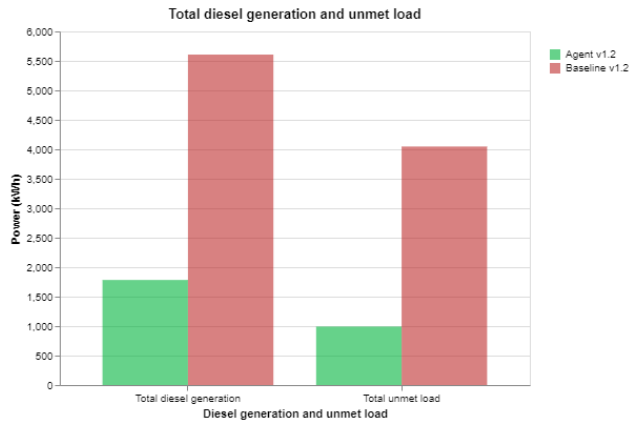


Figure 8.7: Total diesel generation and unmet load in environment v1.2.

### 8.3.2 Implementation of a demand charge and continuous action space.

The implementation of a demand charge posed a challenge in the study. A demand charge is a monthly fee determined by the highest power draw of the month, multiplied by a specified demand rate. This implies that if the agent purchases a large quantity of electricity within one timestep, it would face a hefty demand charge. Hence, the agent must learn to purchase smaller electricity quantities further in advance.

However, the initial RL environment had a flaw. The only action, other than standby, available to the agent was to fully charge its battery within one timestep, leading to significant peak demands. To mitigate this, the introduction of a continuous action space was considered, which would allow the agent to determine any quantity of energy to purchase within a step. The rationale was that this change might encourage the agent to request smaller quantities earlier, thereby charging the battery more gradually during off-peak times.

Despite these expectations, the first attempt with the continuous action space was unsuccessful; the agent struggled to adapt. Several modifications were introduced to the environment to enhance the agent's learning capacity. Primarily, these were recommendations from the stable-baselines3 library [25] designed to aid in model learning. Notably, all values sent to the agent were normalised, the observation space was transitioned from a Dict type to a 1D vector, and a scheduled learning rate was used to train the agent.

To gauge the agent's ability to minimise energy reduction within the continuous space, the demand charge was removed. Following minor bug corrections, the agent adeptly learned to curtail energy expenses using the continuous action space without the constraints of a peak demand charge.

Attempts to implement a rolling demand penalty, which would impose penalties on the agent every time it made large energy purchases, did not yield the intended outcome of prompting the agent to buy smaller energy quantities. In response to this challenge, a more direct approach was taken by capping the agent's energy request capability. A strict upper limit was placed on the energy amount that the agent could request for purchase through the action space. While the rule-based structure remained in place to regulate the microgrid's energy needs, this constraint ensured the agent couldn't

exacerbate the peak demand by making outsized energy requests.

By this phase of development, the RL environment was judged to sufficiently align with the study's complexity scope. The subsequent section offers an in-depth overview of the environment's final version.

## 8.4 Final RL implimentation

This section details the final design of the environment in which the agent learns to manage energy. Additionally, it provides an overview of the training methods of the agent.

### 8.4.1 Environment

The culminating environment incorporates both AC and DC loads, solar PV, and wind generation capabilities, and is equipped with a 500kWh battery and a diesel generator. Furthermore, it integrates loadshedding, TOU rates, and a demand charge.
All input data spans an hourly interval over a year. As detailed in previous sections, data pertaining to loads, generation, time of use rates, and loadshedding history was meticulously amassed. The initial training strategy aimed to utilise the initial 70% of this data as a foundation for the training environment and reserved the subsequent 30% for evaluation purposes. This approach soon presented a challenge.
Notably, figures 8.9 and 8.8 shed light on the disparities inherent in this data split. The winter TOU rates, which are considerably higher than their summer counterparts, are wholly confined to the training environment. Contrarily, the loadshedding data presents an imbalance with 19 instances during training, compared to a staggering 189 occurrences in the evaluation phase.

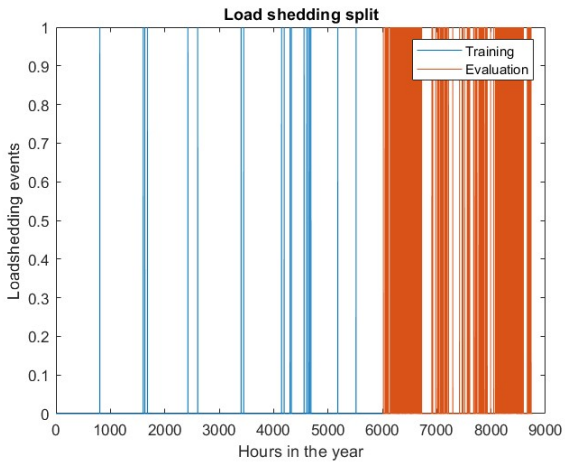


Figure 8.8: Loadshedding events at UCT in 2022.

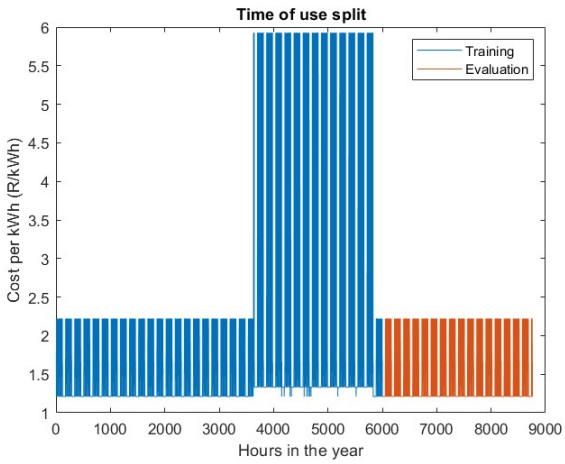


Figure 8.9: UCT's time of use price schedule for 2022.

To rectify the data disparity, the training environment was populated with the first half of each dataset (load, generation, and TOU), while the evaluation environment incorporated the latter half. This strategy aimed to balance the seasonal effects, ensuring the agent was trained on both summer and winter data and subsequently evaluated on similar variations. However, this approach means that only half the data is utilised for training purposes.

The treatment of the loadshedding data deviated slightly from the above method. Given that the first half only recorded 19 loadshedding incidents, it was deemed unsuitable for training. Instead, the more event-rich second half was employed in both the training and evaluation environments.

### 8.4.2 Observation space

The observation space was streamlined while preserving essential information. This design choice aims to mitigate the risk of overloading the agent with excess information that may cloud its ability to learn key relationships.
The final observation space can be seen in listing 8.4.2. Some key changes inlude:

1. All values that were measured in kWh were scaled using the same linear transform to be between the values of -1 and 1.
2. The island_forecast serves as an indicator for loadshedding. A value of 1 signifies the occurrence of loadshedding, whereas a 0 denotes the utility grid's availability.
3. The 'price_forecast' key incorporates the actual TOU tariffs relevant to the current timestep and its forecast window.
4. Initially presented as a Dict type, the observation was flattened into a 1D vector to facilitate more straightforward processing.

```
# Dict space to store all the different observations
self.observation_space = spaces.Dict({
   "power_bal_forecast" : gym.spaces.Box(low=-1, high=1, shape=(1,num_preds), dtype=np.
    ↪ float32),
   "price_forecast"     : gym.spaces.Box(low=0, high=1, shape=(1,num_preds+1), dtype=np.
    ↪ float32),
   "island_forecast"    : gym.spaces.Box(low=0, high=1, shape=(1,num_preds+1), dtype=np.
    ↪ float32),
   "bat_level"          : gym.spaces.Box(low=-1, high=1, shape=(1,), dtype=np.float32),
   "current_power_bal"  : gym.spaces.Box(low=-1, high=1, shape=(1,), dtype=np.float32)
    })
#flatten the observation space to a 1D vector so that it can be interpreted more easily by
    ↪ the agent.
self.observation_space = spaces.flatten_space(self.observation_space)
```

Listing 8.4: Final observation space.

#### 8.4.2.1 SARIMA load forecasts

The load forecasts in the final RL environment are sourced from the SARIMA forecasting model. This model was extensively developed in chapter 6 and evaluated in chapter 7.

Forecasts were structured into a 2D array. Each row of the array corresponds to a timestep in the environment (one for every hour), and the 24 columns represent forecast values for each of the

subsequent 24 hours. A MATLAB script containing the SARIMA model was used to populate this array for every timestep. Subsequently, the forecasts were imported into Python for use in the glsrl environment.

### 8.4.3 Action space

The final action space was a continuous space between -1 and 1. The action that the agent returned was scaled up to be between 0kWh and 200kWh. This was the maximum purchase amount of electricity that the agent was allowed to request to purchase. The upper limit was decided using domain knowledge and an understanding of how much energy would be useful without increasing the peak demand. If the microgrid needs to purchase more power to maintain a positive power balance then it would be able to. The action is only a purchase request and the microgrid is still subject to the rules explained in the step function and outlined in figure B.1. The agent could use the action to preemptively purchase small amounts of electricity and charge its batteries during off-peak hours or in preparation for loadshedding. The finalised action space was set to be a continuous range between -1 and 1. The value of -1 to 1 was selected since the stable-baselines3 library uses a Gausian distribution to calculate the probabilities of taking an action. Scaling the action space to this range is recommended in their documentation[25]. When the agent provides an action, this value gets scaled, spanning from 0kWh to 200kWh — denoting the maximum volume of electricity the agent can opt to purchase.
This upper limit was not arbitrarily set; it was informed by domain knowledge of the microgrid and an understanding of the required purchasing power that would be impactful without unduly elevating peak demand. It's essential to note that this action is not an absolute command. It represents the agent's purchase request, if it is calculated during the step function that more energy is required to maintain a positive energy balance the microgrid will follow its rule-based scheme and purchase additional energy. In this manner, all actions remain constrained by the microgrid rules explained in the step function and depicted in figure B.1.
In operational terms, the agent's action enables strategic energy purchases, allowing for battery charging during off-peak times as a preparatory move ahead of impending loadshedding events or generation shortages.

### 8.4.4 Reward

The final reward structure was designed around four components: purchased energy, diesel generation, unmet load, and peak demand.

- **Purchased Power:** This penalty corresponds to the cost incurred from the electricity purchased during a particular step.
- **Diesel Generation:** This denotes the expenditure associated with utilising the diesel generator. Together, the penalties from purchased power and diesel generation represent the monetary cost per step, as elaborated in listing 8.3.1.
- **Unmet Load:** This component quantifies the unfulfilled load in a given step, scaled by a constant multiplier. Its design aims to add a penalty that reflects any service disruption.
- **Max Demand:** This penalty is structured to motivate the agent towards curtailing its peak demand, thereby reducing the monthly demand charge.

### 8.4.5 Step function

An important function in the final version of the environment was the function that managed the grid. It followed a rule-based system and implemented the agent's actions. As discussed under the action space the agent could request to purchase any amount of energy within the range of 0kWh up to an upper limit set to 200kWh. It manages the power distribution of the AC and DC grid, the grid connection, and the diesel generator. Below is a high-level overview of the method, a more detailed flow chart is seen in figure B.1 in Appendix B.

1. Initial setup:
    - Fetch the AC and DC power balances.
    - Determine the current battery level.
    - Un-normalise the agent's purchase request.
2. Purchase power:
    - Check if the grid is available and purchase the agent-request energy.
    - If the grid is not available no energy may be purchased.
3. Power balance calculation:
    - Compute the total grid power balance using the AC and DC power balance and the additional power purchased.
4. Power allocation:
    - If there is a surplus of energy then the battery is charged with the surplus.
    - If the battery reaches its capacity the remaining surplus is recorded as excess generation.
    - If there is a power deficit then available energy from the battery is used.
    - If the battery reaches its low charge threshold the agent will attempt to purchase electricity from the grid to meet the deficit.
    - If the grid is not available it will use the diesel generator.
    - If the diesel generator does not have sufficient capacity to meet the deficit the remaining deficit will be recorded as unmet demand.

### 8.4.6 Training method

To do

# Chapter 9

# Results & Discussion

## 9.1 Evaluation metrics

The metrics that were used to evaluate the agent's performance were the total monetary cost, the unmet demand, and the amount of diesel generation used. In order to measure the agent's performance, a baseline test was performed. The baseline test entailed simulating the microgrid without requesting to purchase any electricity, meaning that the microgrid would be governed by the rules that were summarised in section 8.4.5 and expanded on in the flow chart found in Appendix B, figure B.1.

## 9.2 Energy management system results

This section outlines the key results that the final energy management agent was able to achieve.

### 9.2.1 Performance of the agent with no loadshedding

The agent has successfully learned to minimise the total cost of purchasing energy in an environment with a stable grid(no loadshedding events), as seen in figure 9.1. The green bars show the performance of the agent while the red bars represent the baseline case.
As seen in figure 9.2 the agent was able to reduce the overall expenditure by purchasing electricity during off-peak times, resulting in overall monetary savings of 5.38%.

Figure 9.1: Total money spent by the agent vs the baseline with a stable grid.

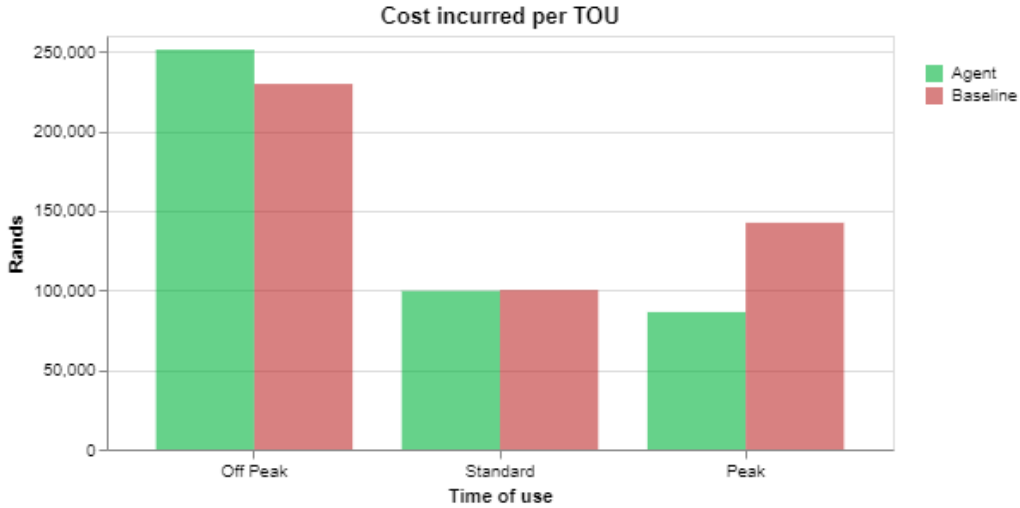


Figure 9.2: Money spent per TOU category.

### 9.2.2 Performance of the agent with loadshedding

In environments that experience an unstable grid and loadshedding, the agent was able to perform even better. It was able to reduce the total monetary expenditure by 6.12% as seen in figure 9.3. As seen in figure 9.5 and 9.4, this reduction in cost was achieved by reducing the amount of money spent during peak times as well as drastically reducing the amount of money spent on diesel generation. The diesel generation is mitigated to an almost negligible 83.18 kWh.

Figure 9.3: The total money spent by the agent vs the baseline case with loadshedding.

The unmet demand was completely eliminated by the agent as seen in the second bar of figure 9.4. Even with a strong incentive to purchase more electricity in order to avoid using the diesel generator or risking unmet demand. The agent was able to find significant savings by purchasing during the off-peak and even the standard TOU categories to avoid purchasing during peak times.

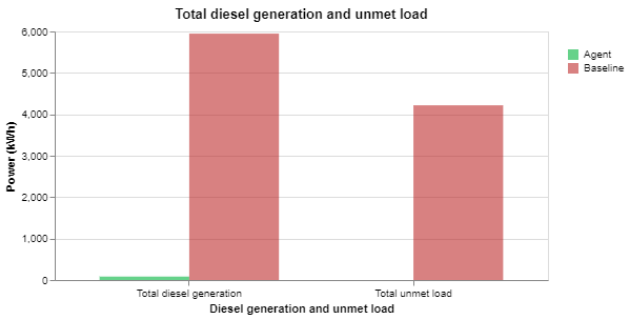


Figure 9.4: Maximum sizing metrics for the hybrid microgrid with loadshedding.

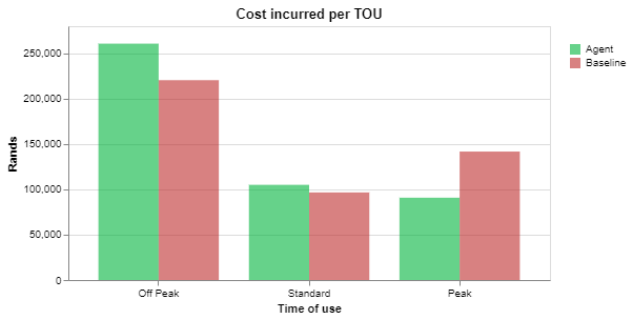


Figure 9.5: The cost of electricity purchased per TOU category with loadshedding.

As expected the total purchased energy was increased by the agent. This is due to the agent purchasing energy before loadshedding events when the grid would be unavailable. This is reflected in the increase of excess generation. The third column in figure 9.6 shows how much of the purchased electricity was requested by the agent. It is slightly less than the actual purchased amount indicating that the agent preferred to under-buy rather than over-buy.

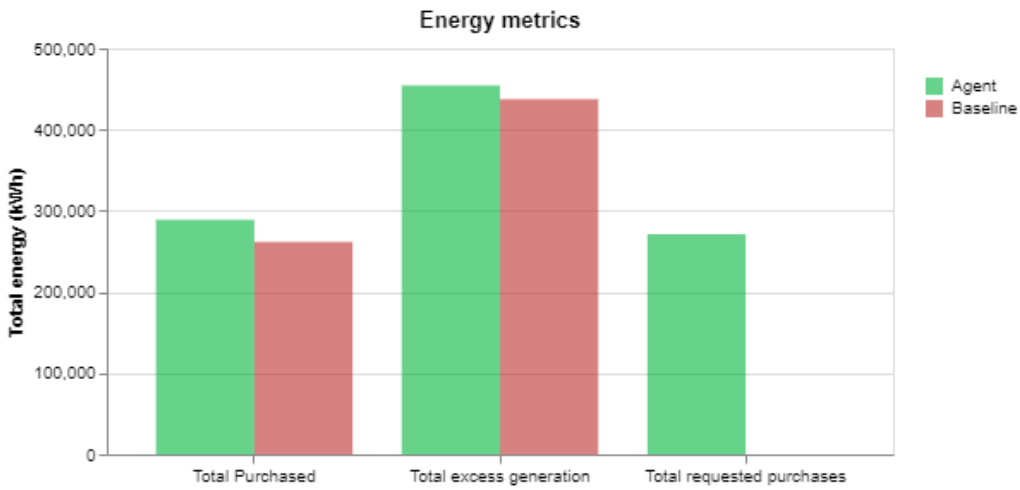


Figure 9.6: The cost of electricity purchased per time of use category with loadshedding.

A summary of all of the important metrics can be found in table 9.2.

| | Total Cost (R) | Diesel Generation (kWh) | Unmet demand (kWh) | Excess Generation (kWh) |
|---|---|---|---|---|
| **No loadshedding** | | | | |
| Baseline | 982392.25 | 0 | 0 | 437520.82 |
| Agent | 929576.61 | 0 | 0 | 441827.28 |
| Percent decrease | 5.38% | NA | NA | -0.98% |
| **With loadshedding** | | | | |
| Baseline | 1023396.93 | 4217.12 | 5947.40 | 437520.82 |
| Agent | 960732.18 | 0 | 83.18 | 454411.43 |
| Percent decrease | 6.12% | 100% | 98.60% | -3.86% |

Table 9.2: Summary of final results

## 9.3 Final energy management discussion

Talk about the final model and its results.

# Chapter 10

# Conclusions and Recommendations

Make sensible recommendations for further work.

# Bibliography


[1] A. K. Barik, S. Jaiswal, and D. C. Das, "Recent trends and development in hybrid microgrid: a review on energy resource planning and control," *International Journal of Sustainable Energy*, vol. 41, no. 4, pp. 308–322, 2022. [Online]. Available: https://doi.org/10.1080/14786451.2021.1910698

[2] S. Moradi, G. Zizzo, S. Favuzza, and F. Massaro, "A stochastic approach for self-healing capability evaluation in active islanded ac/dc hybrid microgrids," *Sustainable Energy, Grids and Networks*, vol. 33, p. 100982, 2023. [Online]. Available: https://www.sciencedirect.com/science/article/pii/S2352467722002272

[3] R. A. Kaushik and N. M. Pindoriya, "A hybrid ac-dc microgrid: Opportunities & key issues in implementation," in *2014 International Conference on Green Computing Communication and Electrical Engineering (ICGCCEE)*, 2014, pp. 1–6.

[4] P. C. Loh, D. Li, Y. K. Chai, and F. Blaabjerg, "Autonomous operation of hybrid microgrid with ac and dc subgrids," *IEEE Transactions on Power Electronics*, vol. 28, no. 5, pp. 2214–2223, 2013.

[5] E. Unamuno and J. A. Barrena, "Hybrid ac/dc microgrids—part i: Review and classification of topologies," *Renewable and Sustainable Energy Reviews*, vol. 52, pp. 1251–1259, 2015. [Online]. Available: https://www.sciencedirect.com/science/article/pii/S1364032115008412

[6] K. Cabana-Jiménez, J. E. Candelo-Becerra, and V. Sousa Santos, "Comprehensive analysis of microgrids configurations and topologies," *Sustainability*, vol. 14, no. 3, 2022. [Online]. Available: https://www.mdpi.com/2071-1050/14/3/1056

[7] B. Naji Alhasnawi, B. H. Jasim, and M. D. Esteban, "A new robust energy management and control strategy for a hybrid microgrid system based on green energy," *Sustainability*, vol. 12, no. 14, 2020. [Online]. Available: https://www.mdpi.com/2071-1050/12/14/5724

[8] Z. Ullah, M. Elkadeem, K. M. Kotb, I. B. Taha, and S. Wang, "Multi-criteria decision-making model for optimal planning of on/off grid hybrid solar, wind, hydro, biomass clean electricity supply," *Renewable Energy*, vol. 179, pp. 885–910, 2021. [Online]. Available: https://www.sciencedirect.com/science/article/pii/S0960148121010673

[9] Z. Ullah, S. Wang, J. Lai, M. Azam, F. Badshah, G. Wu, and M. R. Elkadeem, "Implementation of various control methods for the efficient energy management in hybrid microgrid system," *Ain Shams Engineering Journal*, vol. 14, no. 5, p. 101961, 2023. [Online]. Available: https://www.sciencedirect.com/science/article/pii/S2090447922002726

[10] J. M. Lujano-Rojas, C. Monteiro, R. Dufo-López, and J. L. Bernal-Agustín, "Optimum load management strategy for wind/diesel/battery hybrid power systems," *Renewable Energy*, vol. 44, pp. 288–295, 2012. [Online]. Available: https://www.sciencedirect.com/science/article/pii/S0960148112001243

[11] N. Attou, S.-A. Zidi, M. Khatir, and S. Hadjeri, "Energy management system for hybrid microgrids." *Electrotehnica, Electronica, Automatica*, vol. 69, no. 2, 2021.

[12] S. Kotra and M. K. Mishra, "A supervisory power management system for a hybrid microgrid with hess," *IEEE Transactions on Industrial Electronics*, vol. 64, no. 5, pp. 3640–3649, 2017.

[13] M. Hosseinzadeh and F. R. Salmasi, "Power management of an isolated hybrid ac/dc micro-grid with fuzzy control of battery banks," *IET Renewable Power Generation*, vol. 9, no. 5, pp. 484–493, 2015. [Online]. Available: https://ietresearch.onlinelibrary.wiley.com/doi/abs/10.1049/iet-rpg.2014.0271

[14] A. C. Luna, N. L. Diaz, M. Graells, J. C. Vasquez, and J. M. Guerrero, "Mixed-integer-linear-programming-based energy management system for hybrid pv-wind-battery microgrids: Modeling, design, and experimental verification," *IEEE Transactions on Power Electronics*, vol. 32, no. 4, pp. 2769–2783, 2017.

[15] L. Lv, Z. Wu, L. Zhang, B. B. Gupta, and Z. Tian, "An edge-ai based forecasting approach for improving smart microgrid efficiency," *IEEE Transactions on Industrial Informatics*, vol. 18, no. 11, pp. 7946–7954, 2022.

[16] M. Afrasiabi, M. Mohammadi, M. Rastegar, and A. Kargarian, "Multi-agent microgrid energy management based on deep learning forecaster," *Energy*, vol. 186, p. 115873, 2019. [Online]. Available: https://www.sciencedirect.com/science/article/pii/S0360544219315452

[17] H. H. Aly, "A proposed intelligent short-term load forecasting hybrid models of ann, wnn and kf based on clustering techniques for smart grid," *Electric Power Systems Research*, vol. 182, p. 106191, 2020. [Online]. Available: https://www.sciencedirect.com/science/article/pii/S0378779619305103

[18] Y. Li, R. Wang, and Z. Yang, "Optimal scheduling of isolated microgrids using automated reinforcement learning-based multi-period forecasting," *IEEE Transactions on Sustainable Energy*, vol. 13, no. 1, pp. 159–169, 2022.

[19] H. Musbah, H. H. Aly, and T. A. Little, "Energy management of hybrid energy system sources based on machine learning classification algorithms," *Electric Power Systems Research*, vol. 199, p. 107436, 2021. [Online]. Available: https://www.sciencedirect.com/science/article/pii/S037877962100417X

[20] K. Zhou, K. Zhou, and S. Yang, "Reinforcement learning-based scheduling strategy for energy storage in microgrid," *Journal of Energy Storage*, vol. 51, p. 104379, 2022. [Online]. Available: https://www.sciencedirect.com/science/article/pii/S2352152X22004030

[21] A. Bayas, "Machine learning with matlab." [Online]. Available: https://matlabacademy.mathworks.com/R2023a/portal.html?course=mlml#chapter=5&lesson=4&section=2

[22] Z. Li, F. Liu, W. Yang, S. Peng, and J. Zhou, "A survey of convolutional neural networks: Analysis, applications, and prospects," *IEEE Transactions on Neural Networks and Learning Systems*, vol. 33, no. 12, pp. 6999–7019, 2022.

[23] L. Pauly, H. Peel, S. Luo, D. Hogg, and R. Fuentes, "Deeper networks for pavement crack detection," 07 2017.

[24] Y. Hua, Z. Zhao, R. Li, X. Chen, Z. Liu, and H. Zhang, "Deep learning with long short-term memory for time series prediction," *IEEE Communications Magazine*, vol. 57, no. 6, pp. 114–119, 2019.

[25] A. Raffin, A. Hill, A. Gleave, A. Kanervisto, M. Ernestus, and N. Dormann, "Stable-baselines3: Reliable reinforcement learning implementations," *Journal of Machine Learning Research*, vol. 22, no. 268, pp. 1–8, 2021. [Online]. Available: http://jmlr.org/papers/v22/20-1364.html

[26] F. Angizeh, A. Ghofrani, and M. A. Jafari, "Dataset on hourly load profiles for a set of 24 facilities from industrial, commercial, and residential end-use sectors," 2020.

[27] C. o. Cape Town, "Loadshedding schedule 2018-2023," Sep 2023. [Online]. Available: https://odp-cctegis.opendata.arcgis.com/documents/42551ffb9c494932ac16c4e9cd7dc28e/about

# Appendix A

# Additional Files for Design of Hybrid Microgrid

| **Name of panel** | **Num units** | **Capacity (W)** | **Price (R)** | **Price Per Kw** | **Link** |
|---|---|---|---|---|---|
| Jinko Solar Panel Tiger MonoFacial | 1 | 470 | 1895 | 4031.91 | Link |
| Jinko Solar Panel Tiger Mono-Facial Pallet | 31 | 555 | 67275 | 3910.20 | link |
| JA Solar 144 cell Module | 1 | 465 | 2192 | 4713.98 | Link |
| Canadian Solar 555W Super High Power Mono - Pallet | 31 | 555 | 79143 | 4600.00 | Link |
| Canadian Solar 545W panel | 1 | 545 | 2575 | 4724.77 | Link |

Table A.2: Prices of Solar PV units.

# Appendix B

# Additional information for reinforcement learning implementation

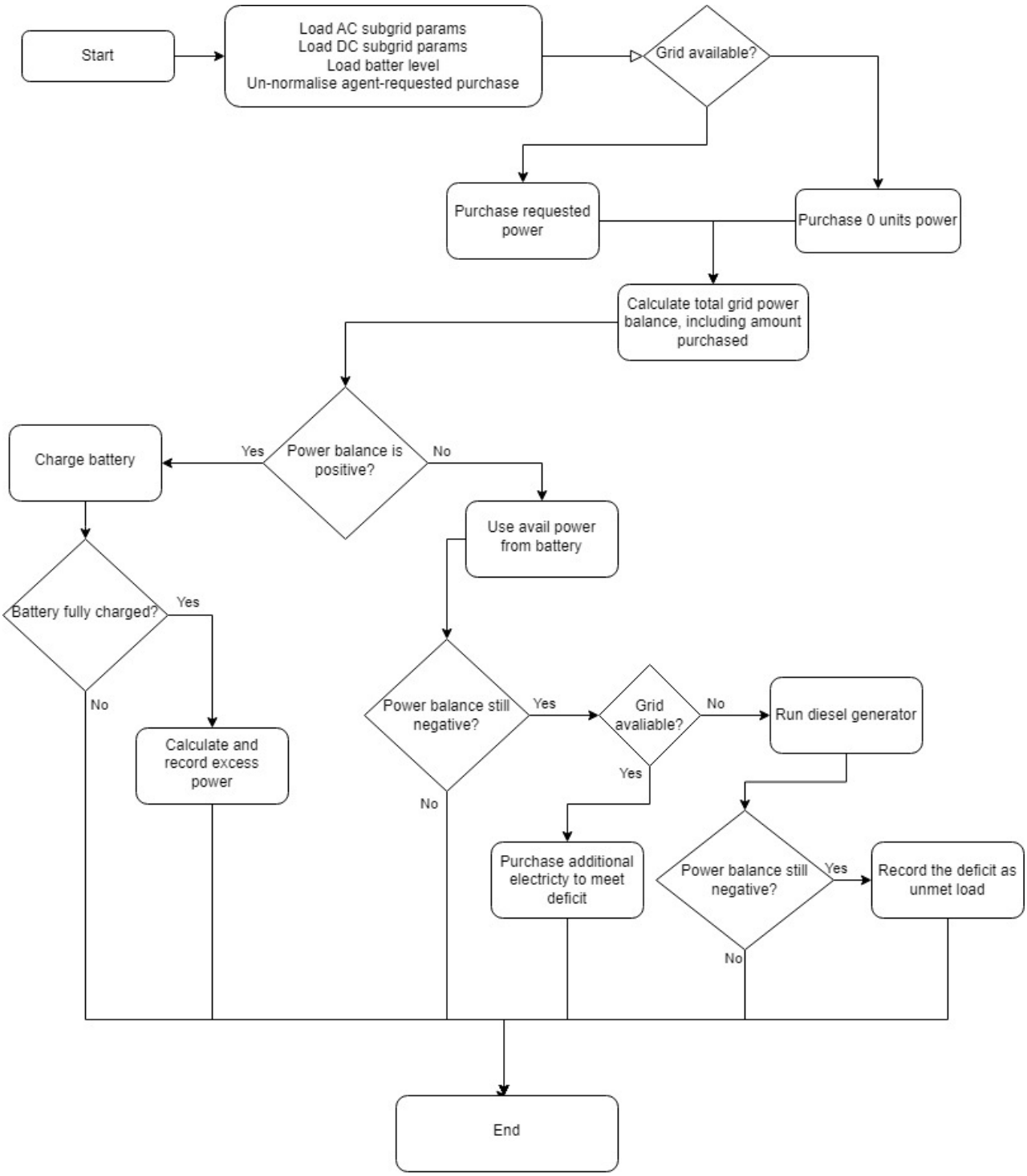


Figure B.1: Rule-based system for management of power in the microgrid

| Version | Additions |
|---|---|
| v0.1 | AC load profile<br>PV Generation profile<br>Time of use indicators (1:Off-peak, 2:Standard, 3:Peak) |
| v0.2 | Changed observation space to hold power balances rather than separate load and generation values (generation - load = power balance). This was done to simplify the observation space. |
| v0.2.1 | Started using Weights and Biases to log results and models.<br>Reduced the number of forecasted steps in the observation space from 24 to 3. This was done to further simplify the observation space. |
| v0.3 | Load shedding, (loadshedding forecasts were included in the agent's observation space so it was aware of oncoming blackouts)<br>Reward structure was modified to include unmet demand with the addition of load shedding<br>the Vec_env wrapper was used to speed up training. |
| v1.0 | Hybrid grid! - AC and DC load<br>Wind turbine profile for AC generation<br>PV array profile for DC generation<br>modified observation space<br>redefined standby and purchase functions to include the new loads and generation forms. |
| v1.1 | Rectifier and inverter power tracking<br>improved logging with Wieghts and Biases. |
| v1.2 | Diesel Generator<br>reward based on real prices<br>included a demand charge in the reward. |
| v2.0 | Introduced a continuous action space to over come demand charge issues. |
| v2.1 | Added intermediate penalty for every purchase that exceeds previous max demand.<br>Included the current max demand in the agents observation space. |
| v2.2 | Scaled the observation space.<br>All the values in kw were normalised with the same scaling function to range -1, 1<br>Time of use rates scaled to range 0,1<br>Action space defined as -1,1 for the agents sampling distributions. Is scaled up to with its own scaling function in the environment. |
| v2.3 | Flattend the observation space to be a 1D vector as it can be processed more efficently.<br>Tested agents with increased learning rates and decreased vf_coef to encourage more exploratory learning. |
| v2.4 | Tested shorter episodes of one month to see if the agent would be learn to predict and avoid the demand charge.<br>Fixed some major bugs with scaling |
| v2.5 | Transition back to normal episode lengths (70% of the year) for training.<br>Removed the demand charge. |
| v2.6 | Cleaned code<br>Working continuous action space (no demand charge) |
| v2.7 | Added structure to use actual forecasts rather than perfect vison<br>Introduced a rolling demand charge penalty |



Table B.2: Version Notes Summary

# Appendix C

# Addenda

## C.1 Ethics Forms